Title: **High efficiency blood-brain barrier transport using a VNAR targeting the Transferrin Receptor 1 (TfR1)**

Authors: Pawel Stocki[§], Krzysztof B Wicher[§], Charlotte LM Jacobsen[¶], Jaroslaw M Szary[§], Mykhaylo Demydchuk[§], Leandra Northall[§], Torben Moos[¶], Frank S Walsh[§] and J Lynn Rutkowski[§*]

[§]Ossianix, Inc, Stevenage Bioscience Catalyst, Gunnels Wood Rd, Stevenage, Herts, SG1 2FX, UK and 3675 Market St, Philadelphia, PA 19104, USA

[¶]Laboratory of Neurobiology, Department of Health Science and Technology, Aalborg University, Fredrik Bajers Vej 3, 9220 Aalborg, Denmark

Address correspondence to:

[*]J. Lynn Rutkowski, PhD

Ossianix, Inc, 3675 Market St., Philadelphia, PA 19104, USA

Email: rutkowski@ossianix.com

Tel: +1(610)291-1724

A one-sentence summary:

Development of highly efficient, TfR1 specific, cross-species reactive blood-brain barrier (BBB) shuttle based on shark single domain VNAR antibody.

Definitions of all symbols, abbreviations, and acronyms:

Transferrin Receptor 1 (TfR1), blood-brain barrier (BBB), Transferrin (Tf), central nervous system (CNS), Variable domain of New Antigen Receptors (VNAR), complementarity-determining region 3 (CDR3), room temperature (RT), size exclusion chromatography (SEC), human serum albumin (HSA), Neurotensin (NT), Immunohistochemistry (IHC), next generation sequencing (NGS), Pharmacokinetic (PK), blood-CSF barrier (BCSFB), Percentage injected dose (%ID), Area under the curve (AUC), attenuated effector function (AEF), sodium dodecyl sulfate polyacrylamide gel electrophoresis (SDS-PAGE), Western blot (WB), intravenous (IV)

ABSTRACT

Transfer across the blood-brain barrier (BBB) remains a significant hurdle for the development of central nervous system (CNS) biologics. We established a functional selection method for BBB-penetrating VNAR antibodies from a synthetic phage library. Combining *in vitro* selection on human TfR1 followed by *in vivo* selection in mice identified the species cross-reactive VNAR TXB2. As a Fc fusion protein, TXB2 binds brain capillaries after intravenous injection and is rapidly transported into the parenchyma and subsequently accumulates in TfR1-positive neurons throughout the brain. Doses of 1.875 mg/kg (25 nmol/kg) produced a rapid, sustained CNS exposure and robust pharmacological activity when fused to neurotensin. There was no was evidence of target-mediated clearance, TfR1 depletion or cytotoxicity as seen with various antibodies to TfR1. This functional selection method for VNARs that can shuttle molecules across the BBB with high efficiency and species cross-reactivity should be widely applicable to other BBB transport systems.

INTRODUCTION

The BBB is formed by highly specialized endothelial cells that maintain an optimal environment for neuronal function by eliminating toxic substances and supplying the brain with nutrients and other metabolic requirements. While the BBB also poses a major challenge for drug delivery to the CNS, receptor-mediated transport systems for endogenous ligands have been exploited to shuttle a wide range of biologics into the brain in a non-invasive manner. TfR1 mediates the transport of iron-loaded transferrin (Tf) from blood to brain and the return of iron-depleted Tf to the blood (*1*). The OX26 monoclonal antibody, which binds the rat TfR1 without blocking Tf and labels capillaries in the rat brain, was the first antibody used to carry a drug across the BBB (*2*). Since then, many biomolecules have been delivered to the brain using a variety of different antibodies to TfR1 (*3*).

Despite clear advances, several features of monoclonal antibodies as BBB carriers have hampered their clinical development. TfR1 antibodies can cause anemia by target-mediated lysis of TfR1-rich reticulocytes (*4, 5*) and off-target binding to TfR1 expressed in other peripheral tissues such as liver and kidney, likely accounts for the relatively short plasma half-life of some TfR1 antibodies (*4, 6, 7*). TfR1 antibodies can accumulate in brain capillaries with limited release into the brain parenchyma (*8*) and target TfR1s in the capillary endothelium for lysosome degradation (*9, 10*). These antibodies have been individually re-engineered to reduce their liabilities and improve brain penetration either by monovalent formatting and/or a reduction in receptor binding affinity (*8, 11-13*). However, these modifications necessitate higher doses to achieve a significant degree of receptor occupancy, and it is not yet clear whether TfR1 transport has been fully maximized for optimal CNS exposure.

Moreover, the TfR1 antibodies used to date bind different epitopes on TfR1 and are species-specific, which remains problematic for preclinical efficacy and safety testing of potential therapeutic molecules.

To address some of the drawbacks with TfR1 antibodies as BBB carriers, we used variable domain of new antigen receptors (VNARs) derived from single chain antibodies found in the shark (*14*). Their unique antigen binding paratope with a long complementarity-determining region 3 (CDR3) provides access to novel epitopes and their small size, high solubility, thermal stability and refolding capacity simplifies coupling to other biopharmaceuticals (*15*). TXB2 was identified from a semi-synthetic VNAR phage display library by a combination of *in vitro* and *in vivo* selection. We show that TXB2 specifically interacts with mouse, rat, monkey and human TfR1 with high affinity (≤1 nM KD) without blocking Tf binding. In mice, TXB2 rapidly crosses the BBB as a bivalent VNAR-human Fc fusion protein (TXB2-hFc), and is readily detected in brain capillaries, parenchyma and neurons at low therapeutic doses (1.875 mg/kg). Neuronal delivery of a biologically active peptide was confirmed at this dose with TXB2-hFc fused to the NT peptide. These results indicated that VNARs to TfR1 have major advantages as BBB carriers without the safety liabilities and poor PK of monoclonal antibodies. Moreover, *in vivo* phage display enables the selection of the rare functionally active VNARs among numerous of TfR1 binders.

MATERIALS & METHODS

***In vitro* phage selections.** Two semi-synthetic libraries were designed to exclude human T-cell epitopes and were based on type I and II nurse shark VNAR sequences (*16*). Phage libraries were produced in super-infected ER2738 cultures and PEG/NaCl precipitated. Two rounds of *in vitro* selection were performed on recombinant hTfR1 ectodomain (Sino Biological) that was biotinylated using Sulfo-NHS-Biotin EZ-Link kit (Thermo Fisher). Streptavidin coupled Dynabeads (Thermo Fisher) were used to pulldown protein-bound phages, which were washed, eluted in 100 nM triethylamine and used for infection of *E. coli* strain ER2738 after adjusting to neutral pH. The output titer was calculated by counting antibiotic-resistant colonies and the culture was super-infected with M13KO7 helper phage to produce phages for subsequent rounds of selection.

Phage ELISA. Individual clones were picked from agar plates and grown at 37°C with shaking in a 96 well block in 2YT media supplemented with 2% glucose, 5 ug/ml tetracycline and 100 μg/ml ampicillin until visible growth occurred. At that point M13KO7 helper phage was added. After 1 hr incubation the media was replaced with 2YT media supplemented with 5ug/ml tetracycline, 100

μg/ml ampicillin and 50 ug/ml kanamycin and grown for 16 hr at 30°C. Plates were then spun down at 2,500xg, the supernatant was recovered and blocked with final concentration of 2.5% milk in PBS with 0.1% Tween20 (PBST) for 15 min at room temperature (RT) before preceding to ELISA. Nunc MaxiSorp plates (Thermo Fisher) were coated with 100 µl of 1 µg/ml of commercially available recombinant mouse and human TfR1 (Sino Biological) and human serum albumin (HSA; Sigma) and incubated at 4°C overnight. Plates were incubated with blocking buffer (2.5% non-fat dry milk in PBST) for 1 hr at RT. Blocked supernatants from phage rescue were transferred to the blocked plates and incubated for 1 hr. The plates were washed with PBST and incubated with anti-M13-HRP 1:3,000 (GE Healthcare) in blocking buffer for 30 min. The plates were washed and developed with SureBlue™ TMB substrate (Thermo Fisher), the reaction stopped with 1% HCl and absorbance measured at 450 nm.

***In vivo* phage selections.** Endotoxins were removed from phage preparations with Triton X-114, which was added to a final concentration of 1% and the preparation was incubated for 5 min on ice followed by 5 min at 37°C. After centrifugation at 13,000 rpm for 5 min at 37°C, the supernatant was transferred to a new tube. The process was repeated twice, and endotoxin levels were measured using the LAL assay (Associates of Cape Cod, Inc.). Female BALB/c mice 6-12 weeks old received a single tail injection of a 100 µl phage preparation ($5x10^{11}$ cfu in PBS), and were then perfused with 25 ml of PBS supplemented with 1 EU/ml of heparin at either 1, 3 and 18 hr after injection. The animals' care was in accordance with institutional guidelines.

Brain fractionation and phage rescue. Brains were removed and the capillaries depleted from the parenchyma as previously described (*17*). Briefly, brain tissue was homogenized with 14 strokes in a Dounce tissue grinder on ice in a 3:1 v/w of physiologic buffer (10 mM HEPES, 141 mM NaCl, 4 mM KCl, 2.8 mM CaCl, 1 mM $MgSO_4$, 1 mM NaH_2PO_4 and 10 mM D-glucose, pH 7.4), and the capillaries depleted by centrifugation through 13% dextran (60-90 kDa) at 5,400xg for 15 min at 4°C. A 1 ml aliquot of supernatant was added to 30 ml of *E. coli* ER2738 cells at mid-log phase growth in 2YT with tetracycline (5 µg/ml). The bacteria were further grown for 2 hr at 37°C while shaken at 250 rpm. After centrifugation at 3,000 rpm for 15 min, the bacterial pellet was plated onto 2YT agar plates containing ampicillin (100 µg/ml) and glucose (2% w/v), and incubated overnight at 30°C. Antibiotic-resistant colonies were counted, and a suspension culture was initiated from the agar plates and allowed to grow to mid-log phase in 2YT media with ampicillin (100 µg/ml) and glucose (2% w/v) before being super-infected with M13KO7 helper phage. The culture was further grown for 1 hr before the media was changed to 2YT with ampicillin (100 µg/ml) and kanamycin (50 µg/ml) and

subsequently grown overnight at 30°C while shaken at 250 rpm. The rescued phages were precipitated with PEG/NaCl and endotoxins were removed before the next round of *in vivo* selection.

Next generation sequencing (NGS). Phagemid DNA samples from each round of selection were prepared using QIAfilter kit (Qiagen). An approximately 350bp region between two *SfiI* restriction sites was sequenced using Illumina MiSeq platform in a 2x250 bp paired-end configuration (GeneWiz). An average Q score of greater than Q30 was obtained for 75% of the sequencing data where Q score refers to log-transformed error probability. The post-acquisition analysis included grouping VNARs into families with common CDR3s using custom written Ruby script. Relative abundance was calculated per million sequences for each stage of the selection using RStudio analysis software.

Production of human Fc and Neurotensin (NT) fusion proteins. Unless specifically indicated all VNAR-hFc formats were produced with VNARs at N-terminal end of human IgG1 Fc and with a series of Fc mutations (E233P/L234V/L235A/ΔG236 + A327G/A330S/P331S) that attenuate effector function (AEF) (*18*). The 8D3-hFc antibody was engineered with VH and VL domains of a rat anti-mouse specific TfR1 antibody (*19*) cloned into human heavy chain IgG1 with AEF and human kappa light chain, respectively. NT constructs were designed to include the peptide on the C-terminal end of hFc with AEF following a 3xG4S linker. For protein production the transient transfection Exp293F expression system (Thermo Fisher) was used following the manufacturer's manual. After 5 day growth, the cells were centrifuged at 2,000 rpm for 10 min. The supernatants were filtered using 0.22 µm membrane filters and loaded onto HiTrap MabSelect SuRe column (GE Healthcare) pre-equilibrated with PBS, pH 7.4. Bound proteins were eluted with 0.1 M Glycine, pH 3.5 and buffer exchanged to PBS, pH 7.4 using HiPrep 26/10 Desalting column (GE Healthcare). Purity of the purified proteins were determined by analytical size exclusion chromatography (SEC) and, if required, protein samples were concentrated and further purified by preparative SEC using a HiLoad 26/600 Superdex 200 pg column (GE Healthcare). Purified proteins were concentrated, filtered using 0.2 µm membrane filters and the quality of the final samples was confirmed by analytical SEC and sodium dodecyl sulfate polyacrylamide gel electrophoresis (SDS-PAGE). The integrity of the NT constructs was confirmed by mass spectrometry.

Production of TfR1 proteins. TfR1 proteins were purified using same expression system as hFc fusion proteins. Expi293F cells were transiently transfected to express His-tagged TfR1 ectodomains of mouse (NP_001344227.1; 123-763aa), rat (NP_073203.1; 123-761aa), monkey (XP_005545315.1; 121-760aa) and human (NP_001121620.1; 120-760aa). Purification was performed on HisTrap Excel

column (GE Healthcare) and if required further purification was done on preparative SEC using a HiLoad 26/600 Superdex 200 pg column (GE Healthcare). Purified proteins were concentrated, filtered using 0.2 µm membrane filters and the quality of the final samples was confirmed by analytical SEC and SDS-PAGE.

Tissue ELISA. Female BALB/c mice 6-12 weeks old were used in the study. The animals received a single intravenous (IV) tail injection of various compounds at doses specific to the experiments described in the results. The animals' care was in accordance with institutional guidelines. MaxiSorp plates were coated with 100 µl of goat anti-human Fc antibody (Sigma) diluted 1:500 in PBS or 3 mg/ml of an anti-VNAR monoclonal antibody (courtesy of Martin Flajnik, University of Maryland, Baltimore) overnight at 4°C. The plates were washed and incubated with blocking buffer for 1 hr at RT. Tissue samples were collected from perfused animal with 25 ml of PBS supplemented with 1 EU/ml of heparin. Brain and peripheral organs were homogenized in 3:1 (v/w) of PBS containing 1% Triton X-100 supplemented with protease inhibitors (cOmplete™, Sigma) using the TissueRuptor (Qiagen) at medium speed for 10 sec and then incubated for 30 min on ice. Lysates were spun down at 17,000xg for 20 min; the supernatant was collected and blocked in 2.5% milk in PBST overnight at 4°C. Blocked brain lysates (100 µl) were added to the blocked plates and incubated for 1 hr at RT. Plates were washed, and the VNAR-hFc concentration determined as described for the binding ELISA.

TfR1 binding ELISA. Nunc MaxiSorp plates (Thermo Fisher) were coated with 100 µl of 1 µg/ml of commercially available recombinant mouse and human TfR1 (Sino Biological), HSA (Sigma), mouse transferrin receptor 2 (TfR2; ACRO Biosystems) or in-house purified monomeric human, mouse, rat, monkey TfR1 and incubated at 4°C overnight. Plates were incubated with blocking buffer (2.5% non-fat dry milk in PBST) for 1 hr at RT. Supernatants from transfected cells or purified proteins were mixed with non-fat dry milk in PBST to a final concentration of 2.5% and incubated for 30 min. The blocked protein solutions (100 µl) were transferred to the blocked plates and incubated for 1 hr. The plates were washed with PBST and incubated with a goat anti-human Fc−peroxidase antibody diluted 1:5,000 (Sigma) in blocking buffer for 30 min. The plates were washed and developed with SureBlue™ TMB substrate (VWR), the reaction stopped with 1% HCl and absorbance measured at 450 nm. The VNAR-Fc concentration was determined from standard curves prepared individually for each fusion protein.

Cell surface expression of TfR1. Exp293F cells (Thermo Fisher) were transiently transfected with pCMV3 plasmids with cloned untagged, full length TfR1 from either mouse (NM_011638.4; Sino Biological MG50741-UT), monkey (NM_001257303.1; Sino Biological CG90253-UT), rat (NM_022712.1; Sino Biological RG80098-UT) or human (NM_001128148.1; Sino Biological HG11020-UT) using ExpiFectamine (Thermo Fisher) following the manufacturer's instructions. The cells were grown overnight in shaking incubator at 350 rpm, 37°C with 8% CO_2 before the transfection reagents were added and the cells were grown for 5 more days. The transfected cells were spun down at 2,000 rpm for 10 min and analyzed by flow cytometry.

Flow cytometry. $2x10^5$ cells/well were transferred into V-bottom 96-well plates. Cells were blocked with PBS containing 1% BSA (FACS buffer) for 10 min on ice and then washed and incubated with TXB2-hFc and either mouse Tf-Alexa Fluor 647 (Jackson ImmunoResearch) or human Tf-Alexa Fluor 647 (Invitrogen) for 30 min on ice. The cells were washed and incubated on ice with secondary antibody anti-hFc-PE (eBioscience) for 20 min in the dark. The cells were washed and resuspended in 200 µl of FACS buffer, and 3 µl of propidium iodide (1 mg/ml) added per well to stain dead cells. The analysis was performed on a CytoFlex flow cytometer (Beckman Coulter).

Competition ELISA. In two variants of the experiment MaxiSorp plates were coated with 100 µl of hTfR1 (Sino Biological) at the concentration of 5 µg/ml overnight at 4°C. Plates were washed with PBST and blocked for 1 hr with 2% BSA in PBST. In the first version of the assay, control wells were left in blocking buffer whereas competition wells were incubated with 2.5 µM Tf for 1 hr and washed before adding 100 µl of TXB2-hFc at the concentration ranging from pM to µM and incubated for 1 hr. In the second version of the assay, biotinylated human Tf (Sigma) at concentrations ranging from pM to µM in 0.1% BSA in PBST was used for pre-incubation for 1 hr before adding 100 µl of TXB2-hFc or human holo-Tf (Sigma) at the concentration of 2.44 nM and further incubated for 1 hr. Following washing, 100 µl of either a 1:5,000 peroxidase-conjugated anti-human Fc antibody or 1:20,000 streptavidin Poly-HRP40 Conjugate (Fitzgerald) diluted in 0.5% BSA in PBST was added and incubated for 1 hr. The plates were washed, and absorbance was measured as for the binding ELISA.

Binding kinetics. Binding kinetics of VNAR-Fcs was determined by surface plasmon resonance (SPR) using a Biacore T200 (GE Healthcare). His capture kit (GE Healthcare) was used to immobilize anti-His antibodies on CM5 chips. In -house purified His-tagged recombinant ectodomain of mouse, rat, monkey and human TfR1 in 0.1% BSA in HBS-EP+ buffer (GE Healthcare) was captured at flow rate 10 µl/min. Analyte binding was measured using the single cycle kinetic SPR method. Analytes including

TXB2-hFc, 8D3-hFc, OX26 (Novus Biologicals), MEM189 (Abcam), OKT9 (Invitrogen) and holo hTf (Sigma) were injected at increasing concentrations (0.98, 3.9, 15.6, 62.5 and 250 nM) in HBS-EP+ at flow rate 30 µl/min. A flow cell without TfR1 captured served as a reference. The chips were regenerated in 10 mM Glycine-HCl, pH 1.5. Sensorgrams were fitted and kinetic constants determined using Biacore T200 Evaluation software (GE Healthcare).

Reticulocytes counts. Mice were injected with compounds as indicated in the results. Blood samples were collected 18 hr post injection and diluted 1:5 with PBS before mixing at 1:100 ratio with 1 ml of BD Retic-Count reagent (BD Biosciences). After a 30 min incubation in the dark at RT, samples were filtered using a cell strainer (35 µm nylon mesh) and reticulocytes counted on a CytoFlex flow cytometer.

Western blotting (WB). To assess changes in TfR1 expression, whole brain lysates were prepared as for ELISAs and the protein concentration determined using a BCA assay (Thermo Fisher). Wells were loaded with 30 µg of total protein, which was resolved by SDS-PAGE under reducing conditions followed by WB onto PVDF membranes. After blocking with 2% BSA for 30 min, the membranes were incubated with mouse anti-TfR1 clone H68.4 (Thermo Fisher) and rabbit anti-actin antibodies (Abcam). After detection with a fluorescent secondary anti-mouse Cy-3 antibody (GE Healthcare), blots were scanned using a Typhoon 5 (GE Healthcare) to quantitate signal intensity using Image Studio Lite (LI-COR Biosciences).

To assess the quality of brain fractionation, the protein concentrations in capillary and parenchymal fractions were measured using the BCA assay kit and 10 µg was loaded per well in reducing buffer without boiling and resolved in SDS-PAGE gel followed by WB into PVDF membrane. After blocking with 2.5% milk for 30 min, the membrane was incubated with rabbit anti-GLUT1 (Abcam) and mouse anti-tubulin (Abcam) antibodies. Signal intensity was determined as for TfR1 above.

Immunohistochemistry (IHC). Sixteen female BALB/c mice, 6 weeks old were acclimatized to local environment conditions for 14 days prior to experiments. The animals' care was in accordance with institutional guidelines (approved under license no: 2018-15-0201-01550 by the Danish Experimental Animal Inspectorate under the Ministry of Food and Agriculture). The mice received a tail vein injection with either control VNAR-hFc or TXB2-hFc in doses of 2 or 12 mg/kg (26.7 nmol/kg and 160 nmol/kg, respectively).

Mice were deeply anesthetized 1 or 18 hr after treatment with a subcutaneous injection of 0.1 ml/10 g of body weight with fentanyl (0.315 mg/ml), fluanisone (10 mg/ml), midazolam (5 mg/ml) in sterile water (1:1:2) and subjected to transcardial perfusion with 0.01M potassium phosphate-buffered saline (PPBS) followed by 4% paraformaldehyde (PFA) in PPBS, pH 7.4. Brains were dissected and post-fixed in 4% PFA at 4°C overnight, extensively washed in PPBS, and then transferred to a 30% sucrose solution for minimum 48 hr. Serial coronal brain sections (40 µm) were cut on a cryostat (Leica CM3050 S), and collected free-floating in PPBS, pH 7.4, in a sequential series of six and stored at -20°C in anti-freeze solution until further processing.

Free-floating brain sections were pre-incubated in blocking buffer (3% porcine serum diluted in 0.01 M PPBS with 0.3% Triton X-100) for 1 hr at RT and then incubated overnight at 4°C with biotinylated goat anti-human IgG antibody (Vector) diluted 1:200 in blocking buffer. After 24 hr, the sections were washed twice in washing buffer (blocking buffer diluted 1:50 in PPBS) and once in PPBS. Antibodies were visualized using the Avidin–Biotin Complex-system (ABC-HRP kit; Vectastain) and 3,3'-diaminobenzidine tetrahydrochloride as the substrate.

Immunofluorescent labelling. For double-fluorescent labeling of TXB2-hFc and endogenous TfR1, sections were co-incubated overnight at 4°C with biotinylated goat anti-human IgG antibody and rat anti-mouse TfR1 (clone RI7217, synthesized by Aalborg University) diluted 1:200 in blocking buffer. Sections were then washed and incubated with Alexa Fluor 594-conjugated donkey anti-rat diluted 1:200 for 30 min (for TfR1) and successively with Avidin–Biotin Complex-system for 30 min, biotinylated-tyramide (diluted 1:100 for 5 min), Avidin–Biotin Complex-system for 30 min, and finally streptavidin-conjugated Alexa Fluor 488 to detect TXB2-hFc. To detect the presence of TXB2-hFc in glial cells, sections were co-incubated with polyclonal rabbit anti-GFAP (Dako) for astrocytes, polyclonal rabbit anti-P25 alpha (courtesy of Poul Henning Jensen, Aarhus University) for oligodendrocytes, or monoclonal rat anti-IBA1 (Serotec) for microglia. The glial marker antibodies were all diluted 1:200 in blocking buffer and detected with donkey anti-rabbit IgG conjugated with Alexa Fluor 594 (1:200, Life Technologies) for 30 min at RT. The fluorescent sections were examined and imaged using the fluorescence DMi8 Confocal Laser Scanning Microscope (Leica).

Body temperature measurements. Five mice per group received tail vein injections with either VNAR-hFc-NT fusions or control hFc-NT at dose from 2.5 to 125 nmol/kg IV (0.2 mg/kg and 9.4 mg/kg) and body temperature was measured over a 24 hr period using a rectal probe, and the data analyzed using Prism software (GraphPad).

RESULTS

VNAR phage display selections. Semi-synthetic VNAR libraries were first subjected to 2 rounds of panning on recombinant hTfR1 ectodomain followed by 3 rounds of *in vivo* selection in mice. The *in vivo* stability of the preselected phage library was tested by injecting $5x10^{11}$ cfu and harvesting perfused brains 1, 3 and 18 hr later. Capillaries were depleted by density centrifugation and the parenchymal fraction was used to infect ER2738 *E. coli*. The phage output titers were determined and approximately 100 clones were randomly picked from each of 1- and 18-hr time points. Binding to human and mouse TfR1 was assessed by phage ELISA. Analysis showed that phage titers in addition to the number of TfR1 binders decreased with time after injection (**Fig. S1A**); thus a 1-hr exposure was used for the subsequent 3 rounds of *in vivo* selections.

The selection process was assessed by NGS where individual clones were identified to amplify in subsequent rounds of selection. Tracking back the 29 most abundant clones from the 3rd round of *in vivo* selection through the entire process that included *in vitro* and *in vivo* stages showed a consistent amplification (**Fig. 1A and Table S1**). However, when the 20 most abundant clones after the *in vitro* stage were tracked forward, only a portion of clones continued to amplify whereas the majority of the clones were de-selected in the *in vivo* stage (**Fig. S1B**). Phage ELISA showed that the number of TfR1 binders increased with each round of *in vivo* selection starting from 5% after round 1 to 15% after round 3 (**Fig. S1C**). There results indicate that the *in vivo* selection process effectively amplified functionally relevant TfR1 binders.

The 29 most abundant clones after the final round of *in vivo* selection (**Table S1**) were re-engineered as bivalent VNAR-hFc fusion proteins to further evaluate their functional activity. Among the 29 clones that were tested, 8 showed TfR1 binding by ELISA, and 7 were cross-reactive to the human and mouse receptor (**Fig. 1B**). The 22 clones that expressed well as VNAR-hFc fusions were tested for brain uptake in mice 18 hr after IV injection at 1.875 mg/kg (25 nmol/kg). A VNAR-hFc that binds TfR1 with nM affinity (**Table S2**) but does not penetrate the BBB was used as a negative control (control VNAR-hFc) throughout the experiments. Brain uptake of TXB2-hFc (clone C) was 14-fold higher than the control and reached 6 nM in the brain 18 hr after injection (**Fig. 1C**). Identical results were obtained using either Fc capture or a VNAR capture ELISAs (**Fig. S2**), which additionally confirmed the integral stability of the fusion molecule upon brain delivery. Two additional clones (E and H) showed a modest increase in brain uptake over the control (4- and 2-fold, respectively), but only clone H bound TfR1.

Binding properties. TXB2 was selected for further characterization. Species cross-reactivity and specificity of this hFc fusion (TXB2-hFc) was tested to the receptor ectodomains, and the full-length receptors expressed on a cell membrane. ELISAs showed binding to mouse, human, cynomolgus monkey and rat TfR1 ectodomain, whereas TXB2-hFc did not bind HSA or mouse TfR2, the nearest homolog (**Fig. 1D**). The binding of TXB2-hFc to human, mouse, rat and cynomolgus monkey TfR1 ectodomains was further analyzed by SPR. TXB2-hFc bound with sub-nM affinity to all but rat TfR1, which measured 1.2 nM KD (**Table S2**) and the binding kinetics were very similar to 8D3, OKT9 and OX26 antibodies which are selective for mouse, human and rat TfR1, respectively. The binding of holo-hTf showed specificity to hTfR1 with a nM KD. The control VNAR-hFc also showed strong nM binding to all but rat TfR1 (**Table S2**) yet unable to penetrate the brain in mice. TXB2-hFc binding to cell surfaces expressing TfR1 (mouse, rat, cynomolgus monkey and human) was assessed in transiently transfected HEK293 cells by double staining for Tf and TXB2-hFc (mouse Tf for cells transfected with mouse, rat and cynomolgus monkey TfR1 and human Tf for cells transfected with human TfR1). Flow cytometry showed that TXB2-hFc bound to mouse, rat and cynomolgus monkey in addition to human TfR1 expressed on the cell surface membrane (**Figs. 1E-F**).

Two ELISAs were setup to test competition between Tf and TXB2-hFc for TfR1 binding. In both variants of the assay plates were coated with human TfR1. In the first variant of the assay TXB2-hFc (at increasing concentrations) showed the same binding to TfR1 alone or when challenged by pre-incubation with Tf at 2.5 µM concentration (**Fig. S3A**). In the second variant of the assay TXB2-hFc (at constant 2.4 nM concentration) showed stable binding to TfR1 when challenged with increasing concentration of biotinylated Tf (bio-Tf) (**Fig. S3B**). Conversely, when bio-Tf binding was challenged with unlabeled Tf, there was observable competition for TfR1 binding, but no competition was detected when TXB2-hFc was used to challenge the binding of bio-Tf (**Fig. S3C**). Thus, no competition between Tf and TXB2-hFc for binding to TfR1 was detected in these molecular assays.

Brain penetration. To further examine BBB transport, capillaries were fractionated from the brain parenchyma and confirmed by WB for GLUT1 (**Fig. 2A**) as a marker specific to cerebral microvessels (*20*). The amount of TXB2-hFc in the parenchyma was more than twice that in capillary fraction by 18 hr after IV injection of 1.875 mg/kg (25 nmol/kg), whereas there was little of control VNAR-hFc in either fraction at the same dose (**Fig. 2B**). In a longitudinal study, the concentration of TXB2-hFc in the capillary fraction was higher than the parenchyma 15 min after injection and then remained relatively constant over a 144 hr study (**Fig. 2C**). In contrast, the parenchymal concentration rose steadily over 18 hr and had only slightly declined by 144 hr. Results from IHC studies provided

further evidence that TXB2-hFc penetrates the BBB into the brain parenchyma after IV injection. TXB2-hFc localized to the capillaries 1 hr after injection and was then visible in the adjacent parenchyma and cellular elements with neuronal morphologies by 18 hr (**Fig. 2D**). TXB2-hFc immunoreactivity within the capillary endothelial cells appeared independent of the dose (2 vs. 12 mg/ml, **Fig. 2D**), which suggested saturation of TfR1s at the BBB.

Brain distribution. TXB2-hFc immunoreactivity was observed in brain capillary endothelial cells, choroid plexus epithelial cells, and neurons after IV dosing (**Figs. 2D, 3 and S4**). Examining the surface of the brain revealed no significant signs of penetration across the pia-arachnoid barrier either after 1 hr (**Fig. S4C**) or 18 hr (**Figs. 3 A, E, H**). TXB2-hFc immunoreactivity was observed in epithelial cells of the choroid plexuses in the lateral, third (**Fig. S4B**), and fourth ventricles. Regions of the brain close to ventricular surfaces were carefully examined for evidence that TXB2-hFc may have crossed the blood-CSF barrier (BCSFB) and entered the brain parenchyma by diffusion. In the diencephalon, faint labeling was seen in neurons of thalamic nuclei, but was unexpectedly absent from the medial habenular nucleus (**Fig. S4B**) known to strongly express TfR1 (*21*). This finding might be attribute to the proximity to the ventricular surface and the flow of the brain interstitial fluid towards the ventricular compartment. Elsewhere in the brain TXB2-hFc immunoreactivity closely mirrored the level of neuronal TfR1 (**Fig.3**), with no indication that neuronal labeling resulted from diffusion into the brain parenchyma from the CSF.

Labeling with TXB2-hFc appeared stronger and more consistent in mice 18 hr after injection with 12 mg/kg, which more clearly illustrates neuronal uptake throughout the brain (**Fig. 3 A-I**). Labeling was highest in neurons of brain stem and cerebellum, but it was also detected in the diencephalon and telencephalic regions. In the neocortex, neuronal labeling was occasionally seen in cortical layers and pyramidal neurons of the hippocampus. In the mesencephalon (**Fig. 3 A, B**), TXB2-hFc immunoreactivity was discernable in reticular formation and cranial nerve nuclei and also seen markedly in neurons of the substantia nigra pars reticulata, more lightly in neurons of the substantia nigra pars compacta, and markedly in the interpedunculate nucleus. In the cerebellum (**Fig. 3 C, D**), TXB2-hFc immunoreactivity was high in Purkinje cells and neurons of deep cerebellar nuclei. In the brain stem (**Fig. 3 E-I**), TXB2-hFc immunoreactivity was prominent in high iron-containing regions and with neurons exhibiting strong TfR1 expression. Such regions include the substantia nigra pars reticulata, deep cerebellar nuclei of the cerebellum, and many neurons of the reticular formation (*21, 22*). The neuronal localization of TXB2-hFc in brain stem regions extended from the medulla oblongata rostrally to the midbrain. In these regions, labeling was particularly high in motor cranial

nerve nuclei and pontine nuclei. Brain sections examined for control VNAR-hFc showed no immunoreactivity in brain capillaries or neurons; however, labeling was seen in choroid plexuses of all ventricles suggesting non-specific transport of this VNAR at BCSFB. Faint immunoreactivity of control VNAR-hFc was confined to the innermost parts of the ventricular surfaces and the surfaces of the brain (**Fig. S4 D-F**) suggesting that BCSFB transport of control VNAR-hFc resulted in very limited diffusion into the brain parenchyma.

Neuronal specificity. Although TXB2-hFc immunoreactivity in brain stem and cerebellum closely mirrored the level of neuronal TfR1 expression as published previously (*21*), double-fluorescent labeling unequivocally confirmed that TXB2-hFc co-localizes with TfR1-postive neurons (**Fig. 3 J-K**). By contrast, TXB2-hFc immunoreactivity was absent in the major glial cell types including astrocytes, microglia and oligodendrocytes (**Fig. S5**). Hence, in pure white matter regions such as the corpus callosum and cerebral peduncle, TXB2-hFc immunoreactivity was only detected in brain capillary endothelial cells.

Biodistribution and safety assessment. The biodistribution of TXB2-hFc was compared to the control VNAR-hFc 18 hr after IV administration of 1.875 mg/kg (25 nmol/kg). The highest absolute concentrations besides plasma were observed in the lung (20-35 nM), followed by similar levels in kidney, heart, liver, spleen (8-18 nM), and the lowest concentration detected in skeletal muscle and brain (**Fig. 4A**). An apparent increase in lung did not reach statistical significance. A significantly higher level of TXB2-hFc relative to control VNAR-hFc was observed only in brain with the increase at nearly 14-fold.

Adverse effects of TfR1 antibodies in mice as a consequence of targeting reticulocytes, which express high levels of TfR1 have been previously reported (*4*). To assess this potential safety liability, TXB2 fusions were produced with a fully functional wild type human IgG1 Fc in addition to AEF variant used throughout this study. Quantitative analysis of reticulocytes in mice injected with 1.875 mg/kg (25 nmol/kg) was performed 18 hr after injection. There was no reduction of circulating reticulocytes in mice injected with TXB2 fused to either wild type or AEF hFc in comparison to animals injected with PBS (**Fig. 4B**).

TXB2-hFc is a bivalent antibody format that binds to mouse TfR1 with 0.63 nM affinity (**Table S2**). It has been reported that high affinity, bivalent TfR1 antibodies are sorted to the lysosome for degradation (*10*) and can reduce TfR1 expression in the brain endothelial cells within a day of

exposure (*9*). To determine whether TXB2-hFc carries a similar liability, mice were injected with TXB2-hFc with AEF at 1.875mg/kg and 18.75mg/kg (25 nmol/kg and 250 nmol/kg). TfR1 levels were quantified by WB after normalization to actin and showed no observable effect on TfR1 expression 18 hr post injection even at the highest concentration (**Figs. 4 C and D**). Importantly, no adverse responses were observed in mice even with the highest dose of TXB2-hFc at 18.75mg/kg (250 nmol/kg).

Pharmacokinetic (PK) profile. The PK properties of TXB2-hFc were further evaluated in time-course and dose-response studies. The PK profile obtained by measuring brain and plasma levels in whole brain extracts after cardiac perfusion was identical to that observed in brain fractionation studies. After a single IV dose of 1.875 mg/kg (25 nmol/kg), the brain concentration of TXB2-hFc increased exponentially over the first 18 hr and then slowly declined over the 144 hr observation period, whereas the slight increase in the concentration of control VNAR-hFc was detected a few hr after injection and remained low over the same period (**Fig. 5A**). Percentage injected dose (%ID) of TXB2-hFc in the brain at 144 hr was calculated at 3% (%ID = brain AUC/plasma AUC x 100%). Although plasma levels of the two fusion proteins diverged in the early redistribution phase, the levels were similar during the elimination phase from 18 to 144 hrs (**Fig. 5B**). In separate PK studies at 1-3 mg/kg, the terminal half-life of TXB2-hFc in plasma was calculated to be 6.5-7 days, which is expected for both human and mouse IgG in mice (*23*).

In dose-response studies, mice were injected IV with 0.1875, 0.75, 1.875 or 7.5 mg/kg (2.5, 10, 25 and 100 nmol/kg) of either TXB2-hFc or control VNAR-hFc and brain levels were measured 18 hr later. The greatest difference between TXB2-hFc and the control VNAR-hFc occurred at the lowest dose (over 35-fold) and exponentially decreased to 8-fold at the highest dose (**Fig. 5C).** Conversely, the plasma levels for the two VNAR fusion proteins were identical for all doses at 18 hr after injection (**Fig. 5D**). In comparison to the 8D3-hFc antibody given at equimolar doses, TXB2-hFc resulted in significantly higher brain (**Fig. 5E**) and plasma concentrations (**Fig. 5F**). At the 25 nmol/kg dose there was over 4-fold more TXB2-hFc in the brain and 6-fold more in the plasma.

Physiological response. TXB2-hFc VNAR was genetically fused to NT peptide, which regulates physiological responses such as body temperature from within the CNS and has been used previously as a measure of parenchymal delivery (*24*). At the 25 nmol/kg IV dose, TXB2-hFc-NT significantly reduced body temperature by >2°C at the 2 hr time point (**Fig. 6A**). Neither of the NT controls (control VNAR-hFc-NT or hFc-NT) produced a significant change at any of the tested time

points. In the dose-response study (**Fig. 6B**), the minimal dose required to produce a hypothermic response at the 2 hr time point was 10 nmol/kg (0.75 mg/kg). Measurement of the brain and plasma concentrations of the NT fusions at the 2 and 24 hr time points showed that TXB2-hFc was 10-fold higher than the NT controls (**Fig. 6C**) and remained constant, despite the reduction of plasma levels over the same time period (**Fig. 6D**). The recovery from hypothermia within 6 hr (**Fig. 6A**) was consistent with the development of receptor desensitization and proteolytic cleavage of the NT peptide (*25*).

DISCUSSION

Previous attempts to identify a brain delivery vehicle using *in vivo* phage display technology targeted the cerebral vasculature (*26-29*), the CSF barrier (*30, 31*) or the olfactory tract (*32*) but not the brain parenchyma. Moreover, the transport mechanism for all of these targeting peptides and antibodies remains unknown. To overcome these drawbacks, we combined an *in vitro* and *in vivo* selection process to isolate cross species reactive VNARs with TfR1 specificity that are transported through the BBB into the brain parenchyma. This was achieved by first selecting VNAR phage libraries on recombinant human TfR1, injecting the pre-selected pool into the bloodstream of mice and then isolating phage clones from the brain parenchyma after capillary depletion. The change in copy number of individual VNAR sequences was tracked by NGS through the multiple rounds of the *in vitro*/*in vivo* selection process.

As anticipated, this two-tiered selection process amplified VNARs that bound both human and mouse TfR1. The most abundant unique sequences at the end of the *in vivo* selection were formatted as bivalent hFc fusion proteins (MW of 75 kDa) to verify brain penetration and mice were treated at a low, therapeutically relevant dose (1.875 mg/kg) to identify the most potent VNARs. TXB2-hFc showed remarkably robust brain uptake, indicating that the selection process effectively identified a highly brain penetrating VNAR through a specific transport mechanism. Subsequent studies confirmed this finding and further defined the biochemical and functional properties of TXB2-hFc and its potential for rapid, efficient and widespread delivery of biologics to the CNS.

TXB2-hFc bound to soluble ectodomains of TfR1 from rat and cynomolgus monkey in addition to human and mouse by ELISA and with affinity similar to that of the reference antibodies OKT9, 8D3 and OX26 against human, mouse and rat TfR1, respectively. TXB2-hFc also recognized the receptor expressed on cell membranes of cells that were transiently transfected with the gene encoding either full-length mouse, human, rat or cynomolgus monkey TfR1. Importantly, TXB2-hFc did not

compete with Tf for TfR1 binding in biochemical assays. These results suggest that TXB2 binds to a surface accessible epitope on TfR1 that is highly conserved and distant from the Tf binding interface. Species cross-reactive antibodies detecting the surface regions of TfR1 are rare, most likely due to genetic divergence at the *TFR1* locus driven by viruses using the receptor for cell entry, which provides a cross-species barriers to virus transmission (*33*). The finding that species cross-reactive VNARs are common could be related to their ability to access buried epitopes.

The interaction of TXB2-hFc with respect to the relationship between TfR1 binding affinity and brain penetration stands in contrast to what has been found with various reference antibodies to the receptor. High affinity binding antibodies to TfR1 appear to impede brain penetration, by retarding transcytosis, lysosomal targeting or preventing the release of the antibody from the receptor into the brain leaving it trapped inside the capillaries (*8, 10, 34-36*). It was further shown that monovalent formatting or lowering the affinity TfR1 antibodies could boost brain transport *in vivo* (*8, 11-13*). Unlike these TfR1 antibodies, a series of biochemical, histological, biodistribution pharmacokinetic and pharmacodynamic studies showed that neither high-affinity TfR1 binding (0.6 nM KD) nor a bivalent format impeded BBB transport of TXB2-hFc.

Brain distribution. The brain distribution of TXB2 expressed as a hFc fusion after IV injection was first examined by biochemical fractionation studies. The results indicate that TXB2-hFc accumulated in the brain parenchyma like TXB2 expressed on the phage surface, thereby validating the *in vivo* phage selection approach. Furthermore, tracking the biochemical distribution of TXB2-hFc after a single dose over time indicates BBB penetration occurs through a rapid, saturable transport mechanism. The time-course study showed that TXB2-hFc levels in the capillary fraction measured 15 min after injection remained constant for at least 144 hr. By contrast, levels in the parenchyma fraction rapidly rose to exceed the capillary levels by 18 hr post-injection and thereafter the two fractions maintained a constant equilibrium throughout the 6-day study. IHC studies confirmed the parenchymal distribution of TXB2-hFc and provide an explanation for the prolonged brain exposure after IV administration.

In addition to the prominent staining of entire microcapillary endothelium, there was also a diffuse widespread staining of the brain parenchyma and specific staining within multiple neuronal populations. The neuronal distribution pattern mirrored TfR1 expression with the most intense TX2B-hFc staining seen in the brain stem and cerebellum, which likely reflects uptake in neurons with highest TfR1 expression (*21, 22*). Double immunofluorescent staining confirmed the co-

localization of TXB2-hFc with TfR1-positive neurons and a striking absence of TXB2-hFc immunoreactivity in astrocytes, oligodendrocytes and microglia, which is in accordance with observations on absence of TfR1 on these major glial cell types (*19, 21*). The extent and intensity of neuronal staining with TXB2-hFc was more robust than previously reported for TfR1 targeted antibodies to date (*8, 11*) and the slow clearance of TXB2-hFc sequestered in neurons most likely accounts for its long half-life in the brain.

Biodistribution. Access of TfR1 antibodies to peripheral tissues though capillary leakage can affect their biodistribution, pharmacokinetics and off-target effects. TfR1 is mainly expressed by cells in the body with high iron demand including lymphoid cells in the spleen, hepatocytes in the liver, myocytes in the heart and skeletal muscle, renal tubules in the kidney and epithelial cells and macrophages in the lung (*1*). After IV injection, the accumulation of TXB2-hFc relative to control VNAR-hFc was only observed in the brain and possibly the lung but not in spleen, liver, heart, skeletal muscle or kidney unlike monoclonal antibodies to mouse TfR1. Interestingly, RI7217 accumulates in the brain and heart but is not taken up by the liver or kidney whereas 8D3 antibody accumulates in liver and kidney in addition to the brain (*6, 7*). Another monoclonal antibody to TfR1 called TSP-A18 preferential accumulated in spleen and bone but not in other mouse organs (*37*). Differences in tissue selectivity by different antibodies indicate that the presentation and availability of TfR1 epitopes for antibody binding is context dependent. TXB2-hFc appears more selective for brain relative to these mouse TfR1 antibodies, suggesting that the TfR1 binding epitope for TXB2 is inaccessible in most peripheral organs and thus less likely to target cargo to peripheral tissues. Additionally, since TXB2-hFc is not targeted to peripheral organs, it is less likely to undergo target-mediated clearance, and which may account for its long plasma half-life relative to other TfR1 antibodies.

Safety profile. TfR1 antibodies have been generated with cytotoxic activity and are being used to target proliferating tumor cells overexpressing the receptor (*38*). To avoid potential toxicity associated with a BBB shuttle, we and others have selected antibodies that do not block the binding of endogenous Tf to its receptor, which could lead to iron deprivation in the CNS (*19*). TfR1 antibodies indirectly prevent iron uptake by interfering with TfR1 recycling and trafficking, which has resulted in lysosomal degradation of the receptor in the capillary endothelium (*9, 10*). Reducing receptor binding affinity and/or monovalent formatting of these antibodies restored intracellular trafficking and maintained TfR1 levels in the CNS. Furthermore, exposure to TfR1 antibodies with full effector function caused severe anemia in mice due to the lysis of TfR1-rich reticulocytes (*4*) and

immune-mediated CNS toxicity in addition to anemia in primates (*5*). However, cytotoxicity related to effector function can be largely attenuated by engineering the antibody Fc region (*4, 18, 39*). TXB2-hFc was evaluated in light of these potential safety liabilities, and we found that it did not block Tf binding, reduce TfR1 levels in the CNS or deplete reticulocytes in mice with or without Fc mutations that mitigate effector function. Since bivalent TfR1 antibodies trigger cellular toxicity by receptor crosslinking (*40*), we suspect that the TXB2 is unable to crosslink the receptor as a bivalent Fc fusion. This finding is in stark contrast to the robust loss of circulating reticulocyte seen with monoclonal antibodies to TfR1 administered at similar doses, which is only partially reversed by the elimination of effector function (*4, 41*). Moreover, certain effector mutations adversely affect plasma and brain PK of the TfR1 antibody and its cargo (*41*), which also was not observed with TXB2-hFc.

Pharmacokinetics. The PK profile of TXB2-hFc is an important distinguishing feature relative to other TfR1 antibodies used as BBB shuttles. Robust brain levels were achieved over an extended period after a single low dose (1.875 mg/kg). The unusually long half-life in the brain can be explained by continuous uptake from plasma via a receptor-mediated transport mechanism and sequestration in TfR1-positive neurons. It should also be noted that measurements of TXB2-hFc in whole brain extracts underestimates the ratio relative to controls since the control VNAR-hFc was not found in the brain parenchyma by IHC. Additionally, there was no evidence of a specific clearance mechanism as the plasma elimination rate of TXB2-hFc was that expected for IgG. By contrast, other high affinity TfR1 antibodies have a short plasma half-life indicative of a target-mediated clearance mechanism; mutations that reduce antibody binding affinity extend the plasma half-life although not to the level of untargeted IgG (*4, 6, 8, 11, 13*). We likewise confirmed the relatively low brain uptake and short plasma half-life of the 8D3-hFc antibody in head-to-head experiments with TXB2-hFc.

While the IHC studies provide strong evidence that TXB2-hFc is principally transported through the BBB pathway, it is possible that BCSFB transport provides a minor contribution to the levels measured in whole brain extracts in our PK studies. Epithelial cells of the choroid plexus express TfR1 in addition to many other transporters found in the BBB and provide active endocytic pathways into the CSF (*42-44*). Additionally, PK studies using microdialysis revealed a nonselective pathway for peripherally administered antibodies into the brain via BCSFB into the ventricles (*45*). The relative contribution of BCSFB pathways to pharmacodynamic effects seen with the therapeutic antibodies delivered to the brain via BBB shuttles warrants further consideration.

CNS activity. Using NT as a cargo has provided a convenient physiological readout to monitor the efficacy of brain delivery (*24*). Endogenous NT is produced by neurons and glial cells within the brain where it functions as a neurotransmitter to regulate a wide array of physiological processes, including body temperature, blood pressure and nociception from within the CNS (*46*). In mice, intracisternal delivery of 10-30 μg NT maximally reduced body temperature within 30 minutes, which returned to near normal 2 hr later (*47*). By comparison, intravenous delivery of NT fused to TXB2-hFc at 1.875 mg/kg (25 nmol/kg) produced a similar reduction in body temperature that peaked 2 hr after administration and returned to normal by 6 hr. The delayed response is consistent with a transit time across the BBB and the extended duration is likely the result of continuous transport in addition to greatly enhanced stability the NT fusion relative to the isolated peptide, which is rapidly degraded (*24*). These two factors likely account for the vastly more potent hypothermic response seen with IV delivery of TXB2-hFc-NT (total dose of <1 nmole into circulation) compared to intracisternal delivery of the isolated peptide (total dose of 6-18 μmoles into the ventricular system). The duration of hypothermia induced by TXB2-hFc-NT would be limited by both CNS tolerance (*48*) and proteolytic cleavage of NT (*25*).

As in the mouse, delivery of NT into the CSF of the rat produced a rapid hypothermic response of a similar magnitude in the same dose range (*47, 48*). As with TXB2-hFc in the mouse, IV delivery in the rat of NT fused to Angiopep-2 (a peptide targeting LDL receptor–related protein-1, LRP1) produced a more potent and extended response than CSF delivery due to the prolonged plasma half-life of the NT fusion protein (*24*). Interestingly, the rapid onset of hypothermia with Angiopep-2-NT closely mimicked the onset of hypothermia after CSF delivery of NT peptide (*47*). Since LRP1 is strongly expressed by choroid plexus cells, transport across the BCSFB may play a prominent role as previously suggested for Angiopep-2 (*44*). Interestingly, the hypothermic potency of TXB2-hFc-NT in the mouse (25 nmol/kg) was 50-fold greater than Angiopep-2-NT in the rat (1.3 μmoles/kg) which may reflect the ability of the TXB2-hFc shuttle to deliver the cargo across the BBB and directly target TfR1-expressing neurons.

In summary, the properties of VNAR TXB2 clearly differ in several important aspects from those of monoclonal antibodies to TfR1 used as BBB shuttles. In contrast to 8D3, OX26, and anti-TfR^{A} (*8*), high affinity binding of TXB2 to TfR1 did not impeded transport across the BBB. Subsequent to capillary binding, TXB2-hFc widely distributed across the brain and was internalized by TfR1-expressing neuronal populations. Moreover, the pharmacokinetic profile of TXB2-hFc was distinguished by prolonged brain exposure and the lack of target-mediated clearance. Consequently, the minimal

effective doses of TXB2-hFc fused to NT was as low as 1-2 mg/kg (12.5-25 nmol/kg), indicating the shuttle is capable of highly efficient BBB transport. The favorable properties of TXB2 as a BBB shuttle could be due to the inherent binding properties of the VNAR, the particular epitope on TfR1 to which it binds or functional selection *in vivo*, or a combination of these. Since VNAR TXB2 represents the primary hit from the *in vivo* selection approach, further improvements in BBB transport are possible to optimize this VNAR for therapeutic development.

Acknowledgments

The authors wish to thank Martin Flajnik for valuable insight into the VNAR single domain and Hanne Krone Nielsen and Merete Fredsgaard for excellent technical assistance.

Conflict of interest

P.S., K.B.W., J.M.S., M.D., L.N., F.S.W., J.L.R. were paid employees of Ossianix Inc.. Ossianix Inc. filled patents on the subject matter of this manuscript. C.L.M.J. and T.M. work was supported by grants from the Lundbeck Foundation Research Initiative on Brain Barriers and Drug Delivery (Grant no. R155-2013-14113).

Figure 1

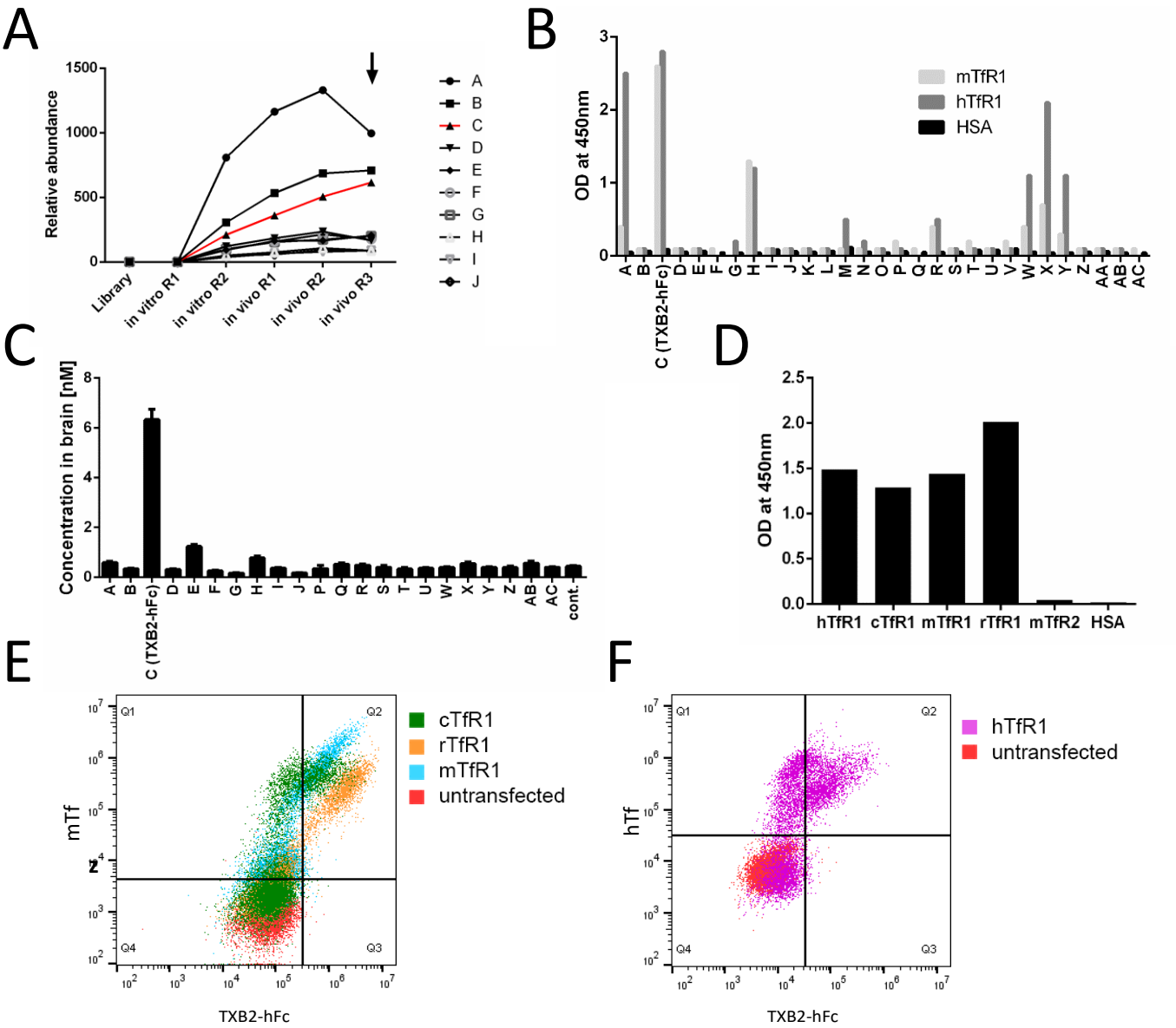

Figure 1. Selection, TfR1 binding and brain uptake of selected VNAR clones. (**A**) The selection process was monitored by NGS and the relative abundance of each VNAR family (CDR3-grouped) per million sequences was calculated. The progressive enrichment of the 10 most abundant clones (Table S1) from *in vivo* round 3 (marked by arrow) was represented in earlier rounds of selection. (**B**) Relative ELISA binding of the 29 most enriched VNARs (Table S1) formatted as hFc fusions to human TfR1 (hTfR1) and mouse TfR1 (mTfR1). (**C**) Brain concentration of the 22 tested VNAR-hFc fusions 18 hr after single IV injection of 1.875 mg/kg (25 nmol/kg) as determined by ELISA (mean ±SD, N=5). Control VNAR-hFc that binds to TfR1 (Table S2) was included as negative control (cont.). (**D**) Comparative ELISA binding of TXB2-hFc to recombinant hTfR1, mTfR1, cynomolgus monkey (cTfR1), and rat (rTfR1), with mouse TfR2 (mTfR2) and HSA as negative controls. Live HEK293 cells transiently transfected with (**E**) mTfR1, cTfR1, rTfR1 or (**F**) hTfR1 were co-stained with TXB2-hFc and either transferrin from mouse (mTf) or human (hTf) and analysed by flow cytometry. Double-positive cells that populated Q2 after transfection showed binding of both TXB2-hFc and Tf to the transiently expressed TfR1.

Figure 2

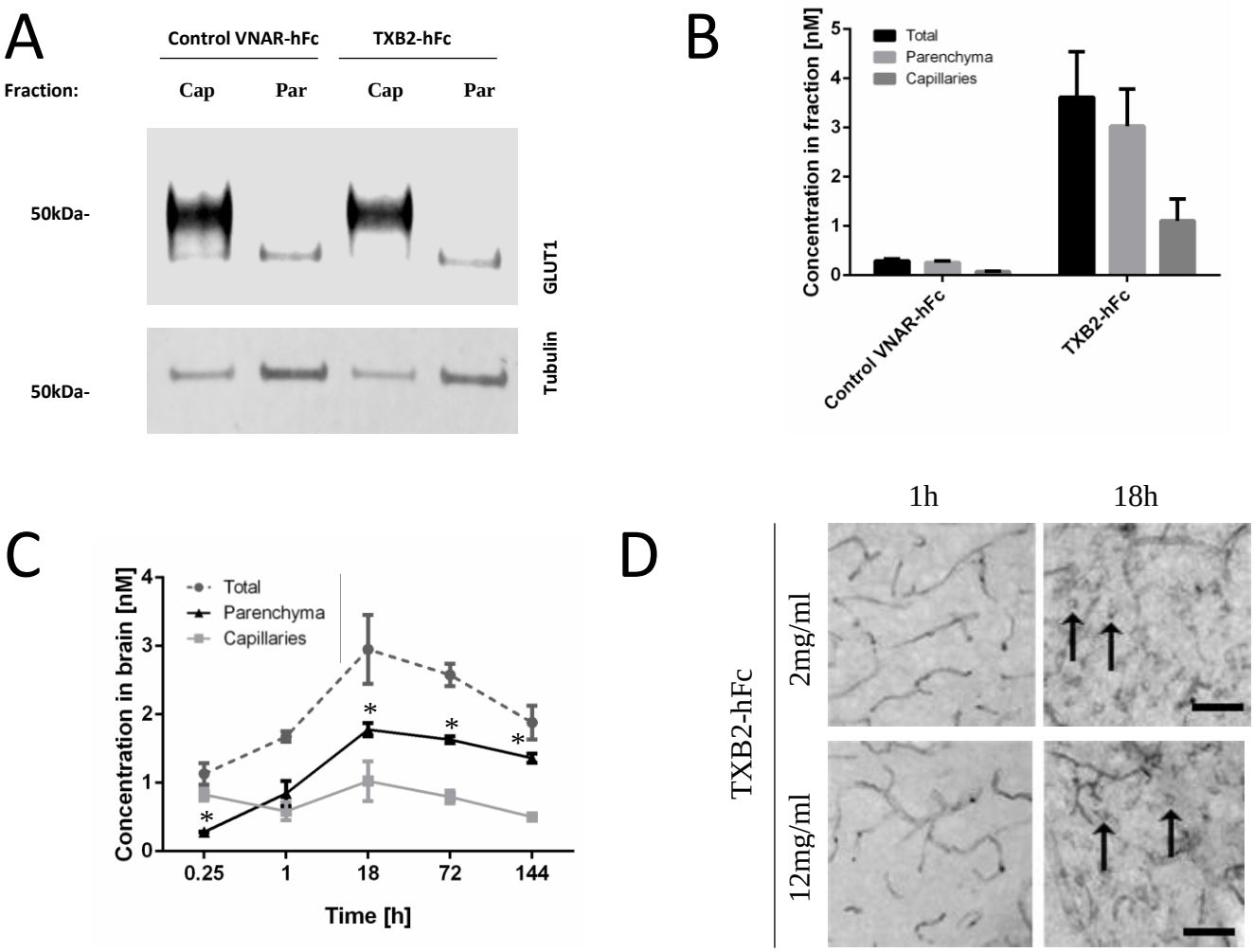

Figure 2. Parenchymal distribution of TXB2-hFc in brain after IV injection. (**A**) WB of capillary and parenchymal fractions. Separation of capillary (Cap) and parenchymal (Par) fractions after density centrifugation was shown by SDS-PAGE followed by WB for GLUT1 (capillaries) and tubulin (loading control). (**B**) Mice were administered TXB2-hFc or control VNAR-hFc at 1.875 mg/kg (25 nmol/kg) IV and VNAR-Fc concentrations in the capillary and parenchymal fractions compared to the unfractionated contralateral hemisphere (total) (mean ±SD, N=3). (**C**) Concentrations of TXB2-Fc in brain fractions over time after a single IV injection of 1.875 mg/kg (mean ±SD, N=3). * Indicates significant difference between parenchymal and capillary fractions ($p < 0.05$) by Student's t-test. (**D**) Brain section from the superior colliculus of the mesencephalon. TXB2-hFc was injected at 2 or 12 mg/kg and allowed to circulate for 1 or 18 hrs. Immunolabeling was restricted to brain capillaries at 1 hr but after 18 hr additional parenchymal staining was observed; cells with a neuronal morphology were marked (arrows). Scale bar 50 µm.

Figure 3

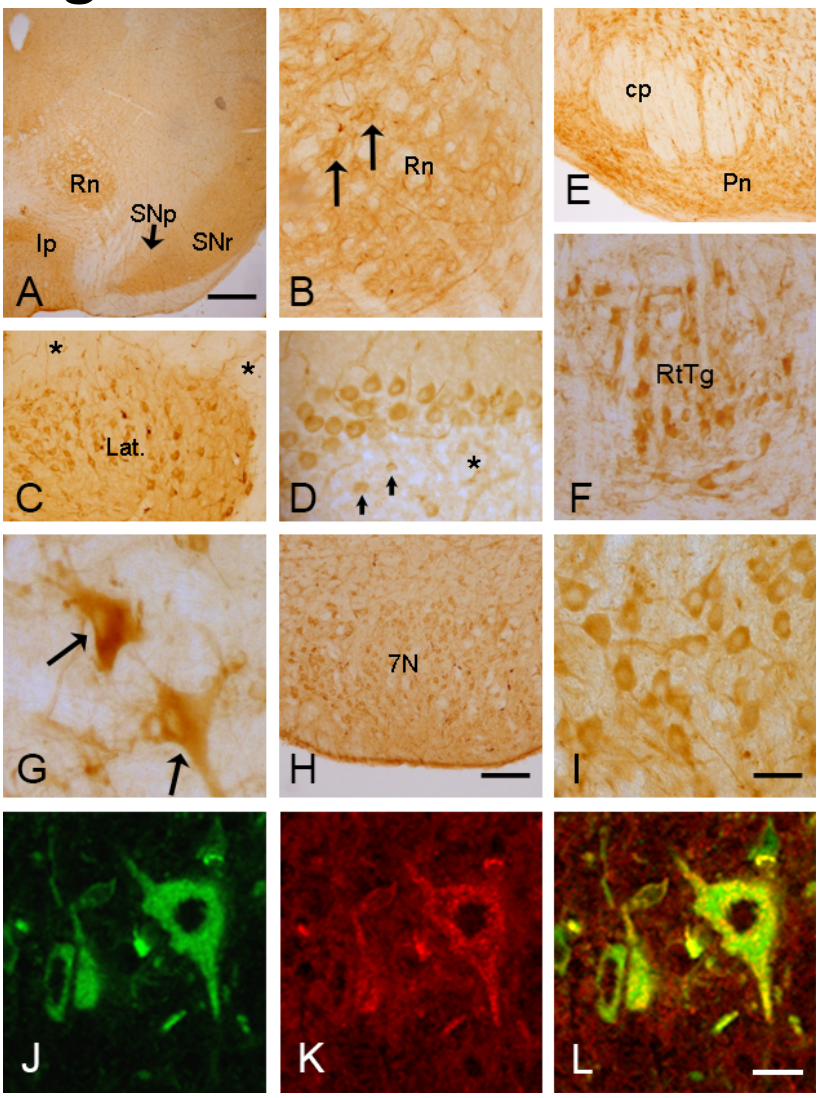

Figure 3. The distribution of TXB2-hFc in brain stem and cerebellum. IHC brain tissue analysis 18 hr after a dose of 12 mg/kg IV. The mesencephalon (**A**), with the red nucleus (Rn), interpedunculate nucleus (Ip), substantia nigra pars compacta (SNp) and substantia nigra pars reticulata (SNr). The Rn is shown in higher magnification (**B**) with neurons (arrows). The cerebellum (**C, D**), with the lateral nucleus (Lat.) and Purkinje cells (**D**), with discrete granular cells (arrows) and brain capillaries (*). The lower brain stem (**E-I**), with the reticular formation and cranial nerve nuclei. The pons (**E**) with the pontine nucleus (Pn), white matter-rich cerebral peduncle (cp) and neuronal labeling in the reticulotegmental nucleus (RtTg) (**F**). (**G**) Neuronal labeling is prominent in the reticular formation (arrows). (**H**) Labeling of neurons of the facial nucleus in lower and (**I**) higher magnification**.** Double fluorescent images taken in upper brain stem showing labeled neurons of the red nucleus. Neurons stained for (**J**) TXB2-hFc (green) and (**K**) TfR1 (red). (**L**) Merge image with green and red channels overlay showing double-labeling in yellow. Scale bars: **A** 1 mm, **B-D,F,I** 50 µm (bar shown in I), **E,H** 200 µm (bar shown in H), **G,J-L** 5 µm (bar shown in L).

Figure 4

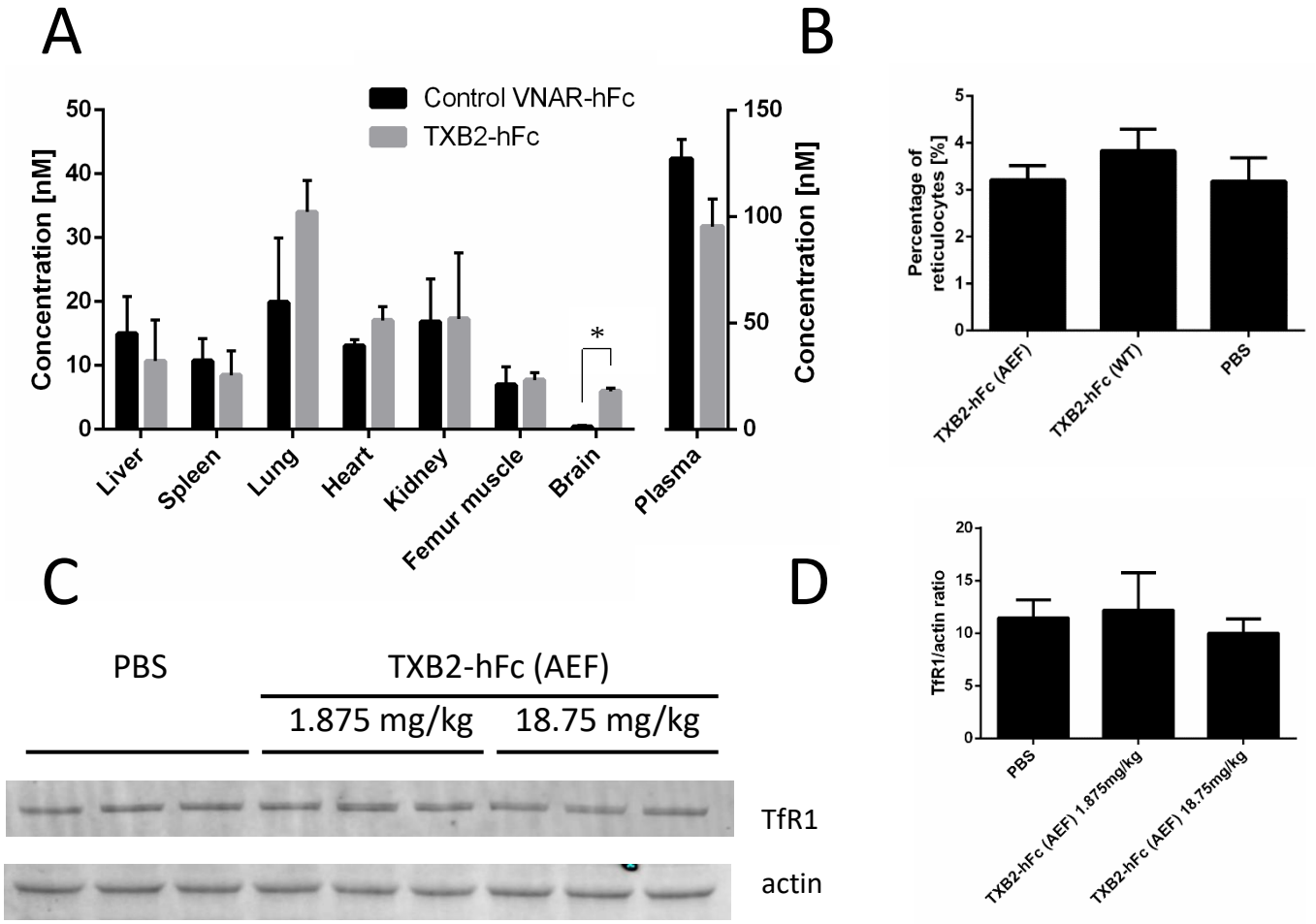

Figure 4. Biodistribution of TXB2-hFc and effect on circulating reticulocyte count or TfR1 expression in brain. (**A**) Biodistribution of TXB2-hFc compared to control VNAR-hFc in mouse liver, spleen, lung, heart, kidney, femur muscle, brain and plasma. Organs were collected 18 hr post IV injection at 1.875 mg/kg (25 nmol/kg) dose. The samples were homogenized and quantified using ELISA (mean ±SD, N=3). * Indicates significance ($p < 0.01$) by Student's t-test. (**B**) TXB2 fused to hFc with attenuated effector function (AEF) or fully functional wild type (WT). Mice were injected IV at 1.875 mg/kg (25 nmol/kg). Blood samples were collected 18 hr post injection and percentage of reticulocytes in total number of red cells (mean ±SD, N=3) was determined by flow cytometry after staining with Thiazole Orange. (**C**) TXB2-hFc (AEF) at a dose of 1.875 or 18.75 mg/kg (25 or 250 nmol/kg) was injected IV and perfused brains were harvested 18 hr later. Brain homogenates were analysed by SDS-PAGE followed by WB using fluorescently labelled antibodies to detect TfR1 and actin. (**D**) WB data presented as a ratio of the TfR1 to actin signal (mean ±SD, N=5).

Figure 5

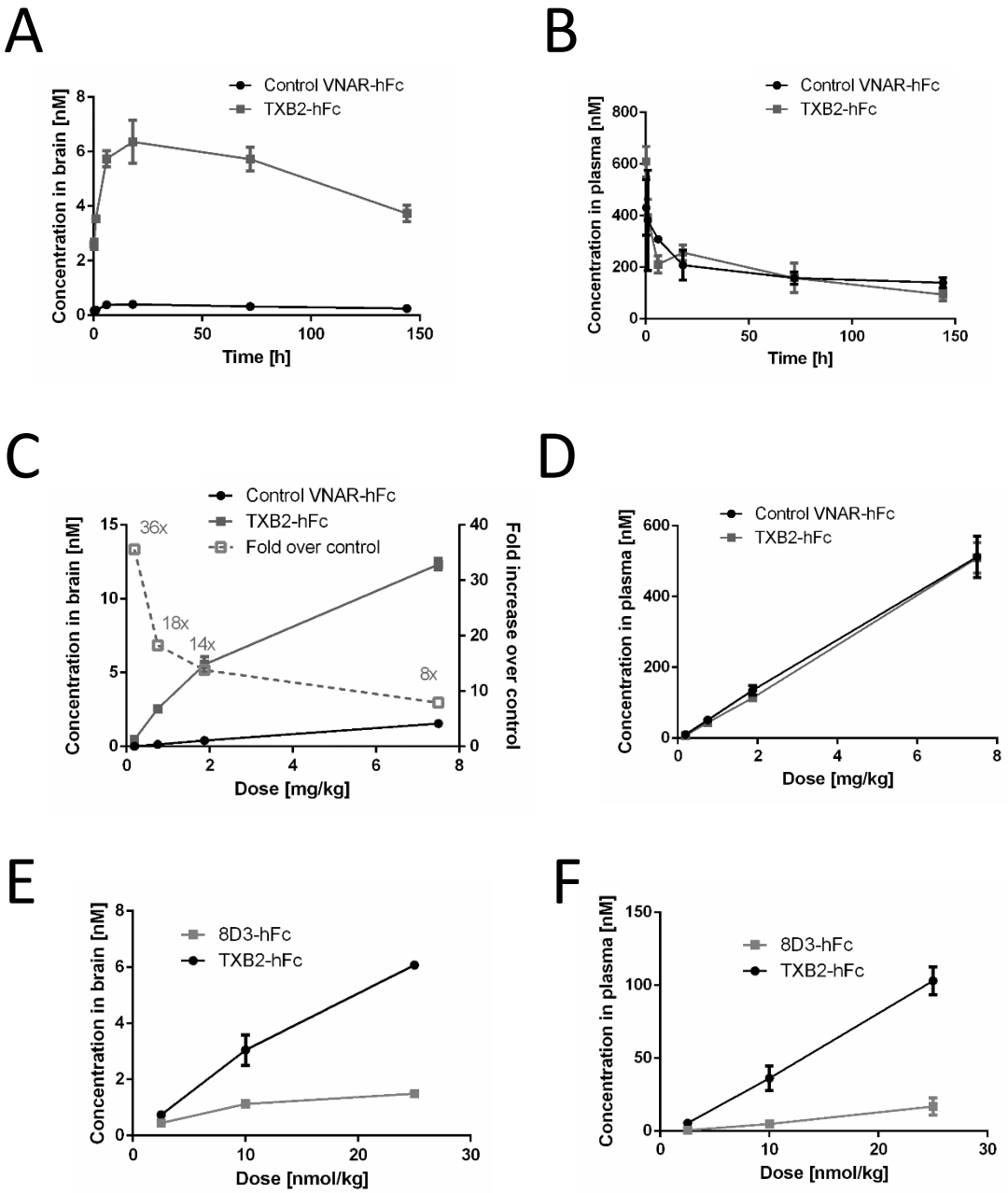

Figure 5. Transport kinetics of TXB2-hFc in brain after IV injection. The time course experiment with concentrations in brain (**A**) and plasma (**B**) of TXB2-hFc or control VNAR-hFc after single IV injection of 1.875 mg/kg (25 nmol/kg). Dose-response curves showing brain (**C**) and plasma (**D**) concentrations 18 hr after IV injection of TXB2-hFc or control VNAR-hFc with the fold over control indicated (dashed line) at each dose. Dose-response curves showing brain (**E**) and plasma **(F)** concentrations of TXB2-hFc compared to 8D3-hFc injected at molar equivalent doses. All tissue concentrations determined by an Fc-capture ELISA (mean +SD, N=4-5).

Figure 6

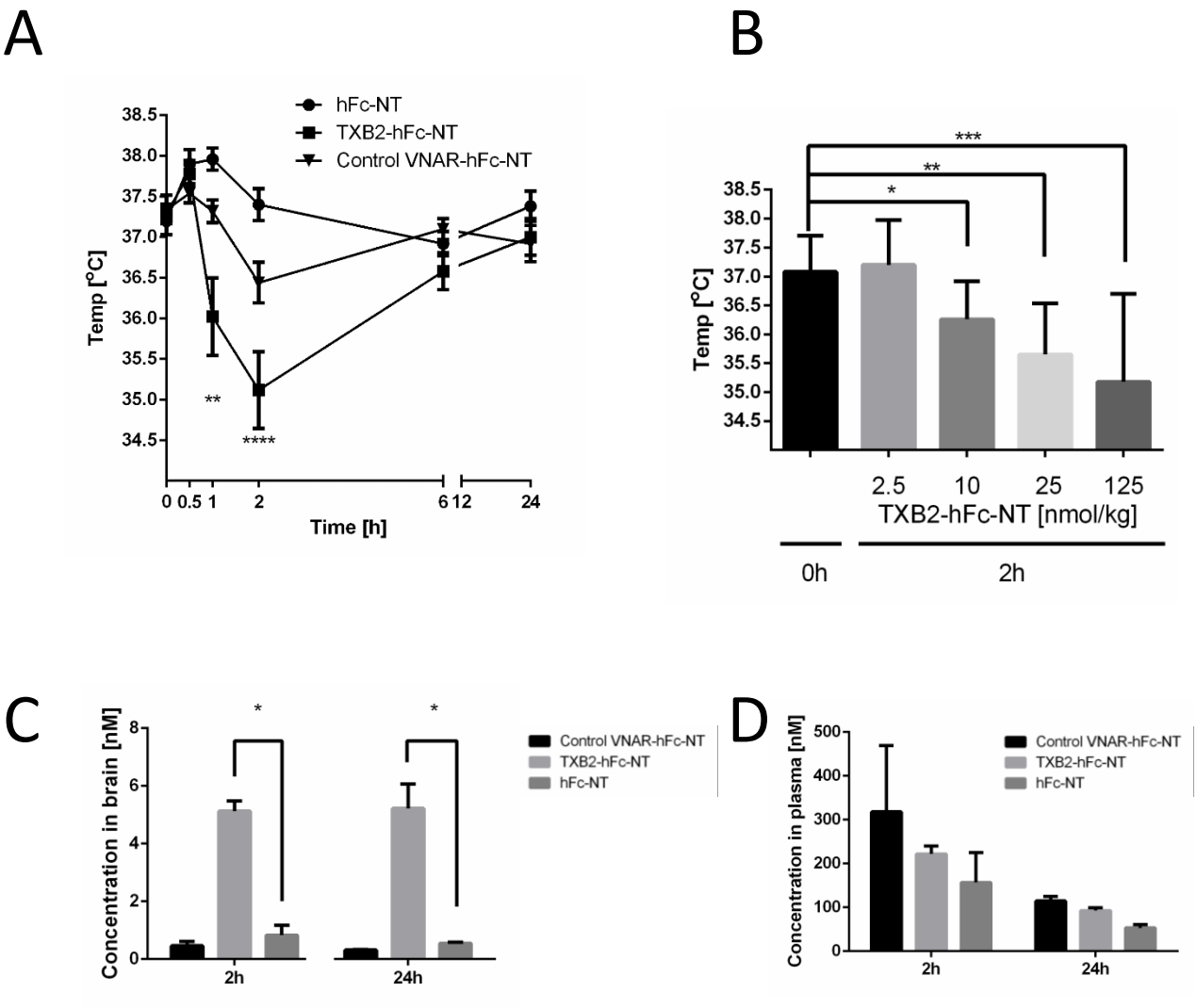

Figure 6. Body temperature decrease after TXB2 delivery of neurotensin (NT) to the brain. The NT peptide was genetically fused to the C-terminus of tested constructs. (**A**) Mice were injected IV with VNAR-hFc-NT fusions or hFc-NT control at 25 nmol/kg and body temperature measured over 24-hr period (mean ±SD, N=5). Significance at **-p<0.01 and ****-p<0.0001 by two-way ANOVA with Dunnett's comparison test. (**B**) Dose-dependent hypothermia induced by TXB2-hFc-NT measured at 2 hr (mean ±SD, N=5). Significance at *-p<0.05; **-p<0.01; ***-p<0.001 determined by the Mann-Whitney test. Brain (**C**) and plasma **(D)** concentrations of the NT fusion constructs were measured by ELISA after 2 hr (N=3) and 24 hr (N=5). * Indicates significant (p< 0.01) by Student's t-test.

Supplementary Material
Figure S1

A

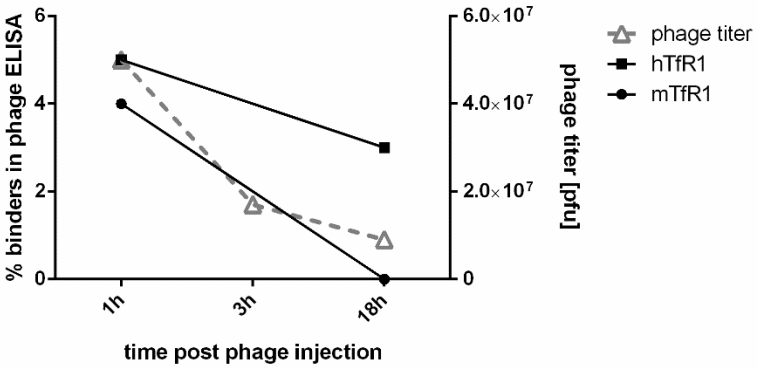

B

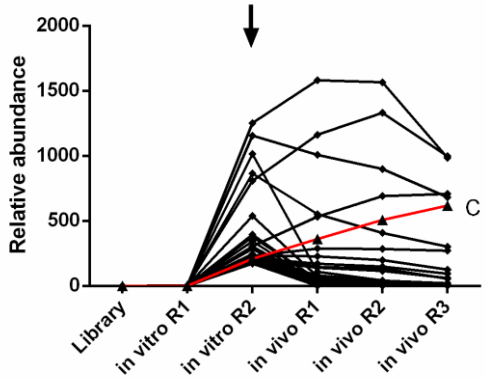

C

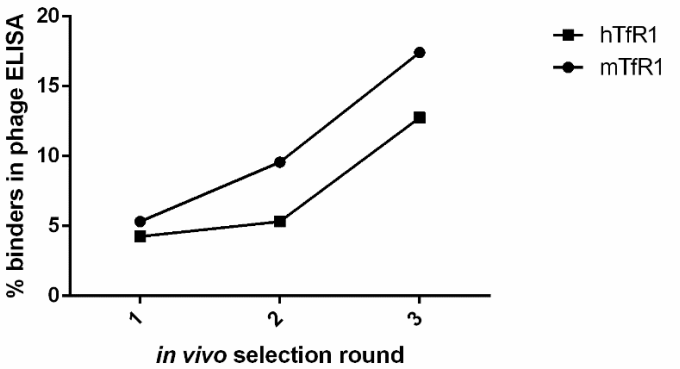

Figure S1. In vitro/in vivo selection of brain penetrant VNARs. (**A**) Optimization of *in vivo* selection method for TfR1-dependent brain penetrants. Preselected phage library was injected to animals and the brains were extracted 1, 3 or 18 hr post injection following cardiac perfusion. The phage output titer was calculated using plaque-forming unit (pfu) in parenchymal fraction only. Approximately 100 clones were randomly picked from 1- and 18-hr time-points and binding to human (■) and mouse (•) TfR1 was assessed by phage ELISA. (**B**) The 20 most abundant sequences at the 2nd *in vitro* round of selection (marked by arrow) were tracked for their abundance in the further rounds of *in vivo* selection. (**C**) Individual clones were randomly picked and tested in phage ELISA for binding to human and mouse TfR1 (hTfR1 and mTfR1). Approximately 200 clones were picked for each of rounds 1 and 2, and 800 clones were picked for round 3. A clone was defined as a binder if its signal exceeded four times the background signal.

Figure S2

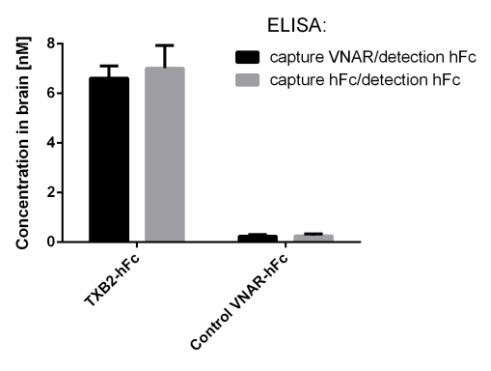

Figure S2. Stability of the VNAR-Fc format in brain was subsequently assessed by using alternative two ELISAs with Fc-capture or VNAR-capture with the same Fc detection antibody (mean ±SD, N=3).

Figure S3

A

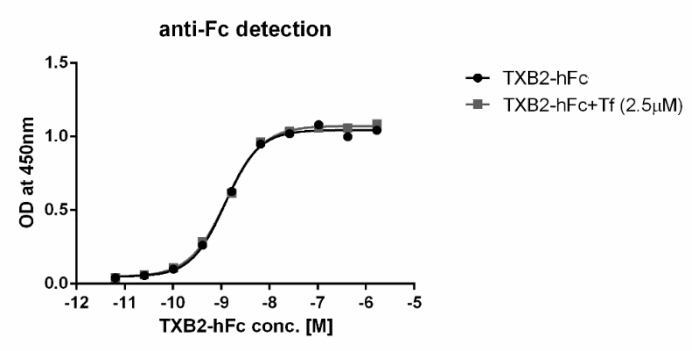

B

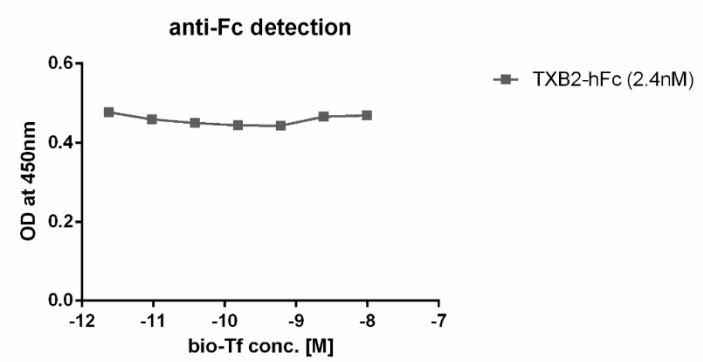

C

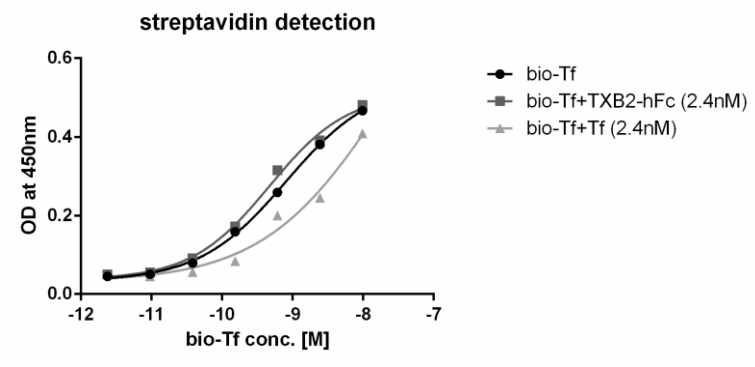

Figure S3. Competition analysis between TXB2-hFc and Tf for binding to TfR1. ELISA plates were coated with recombinant hTfR1. (**A**) Binding of TXB2-hFc to hTfR1 at concentrations ranging from pM to µM was assessed on its own and after pre-incubation with 2.5 µM of recombinant Tf. (**B** and **C**) Alternatively, plates were pre-incubated with biotinylated Tf (bio-Tf) at concentrations ranging from pM to µM. After the addition of either TXB2-hFc or unlabeled Tf (both at 2.4 nM), TXB2-hFc binding was detected with anti-human Fc antibody (**B**) and bio-Tf with streptavidin (**C**).

Figure S4

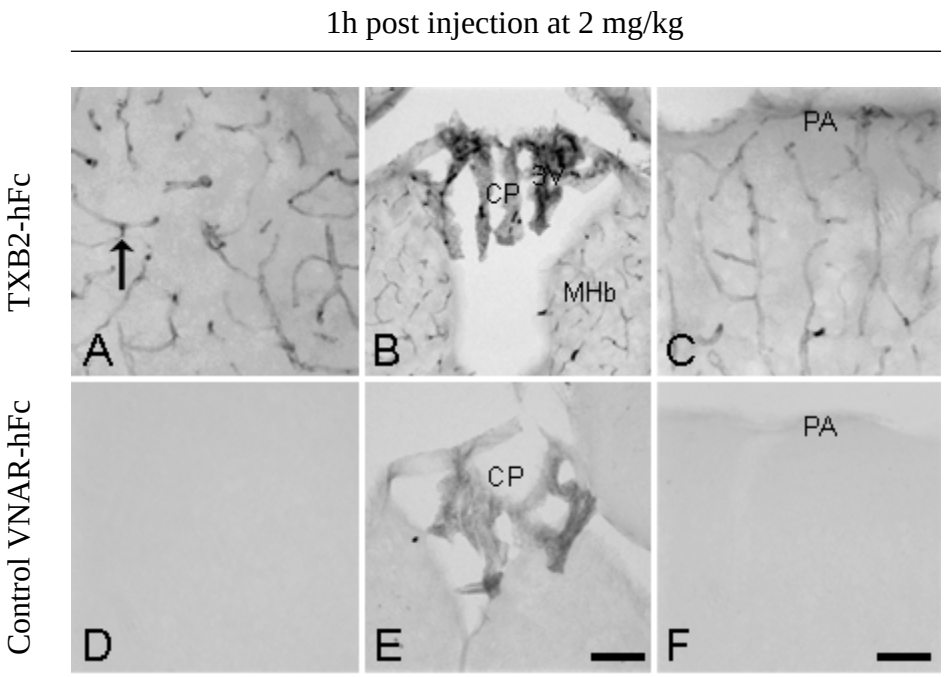

Figure S4. The brain distribution of TXB2-hFc as evaluated using IHC. (**A-C**) TXB2-hFc injected in a dose of 2 mg/kg, IV and allowed to circulate for 1 hr. (**A**) TXB2-hFc is present in brain capillaries (arrow) throughout the brain. (**B)** Labelling is also seen in the choroid plexus (CP), but not in the adjacent brain tissue containing the medial habenular nucleus (MHb) lining the third ventricle (3V). (**C)** In the cerebral cortex and the surface of the brain, labelling is confined to brain capillaries and is not prominent at the level of the pia-arachnoid membrane (PA). (**D-F**) Control VNAR-hFc injected at a dose of 2 mg/kg and allowed to circulate for 1 hr. (**D**) Labelling is virtually absent and does not discern any pattern of labelling in brain capillaries. (**E**) Labelling is nonetheless seen in the CP, which can be attributed to non-specific transport at the BCSFB. (**F**) Labelling is virtually absent from the PA, indicating that the amount of control VNAR-hFc transported into the brain is low. Scale bars: **A, C, D, F** 50 µm (bar shown in **F**), **B, E** 200 µm (bar shown in **E**).

Figure S5

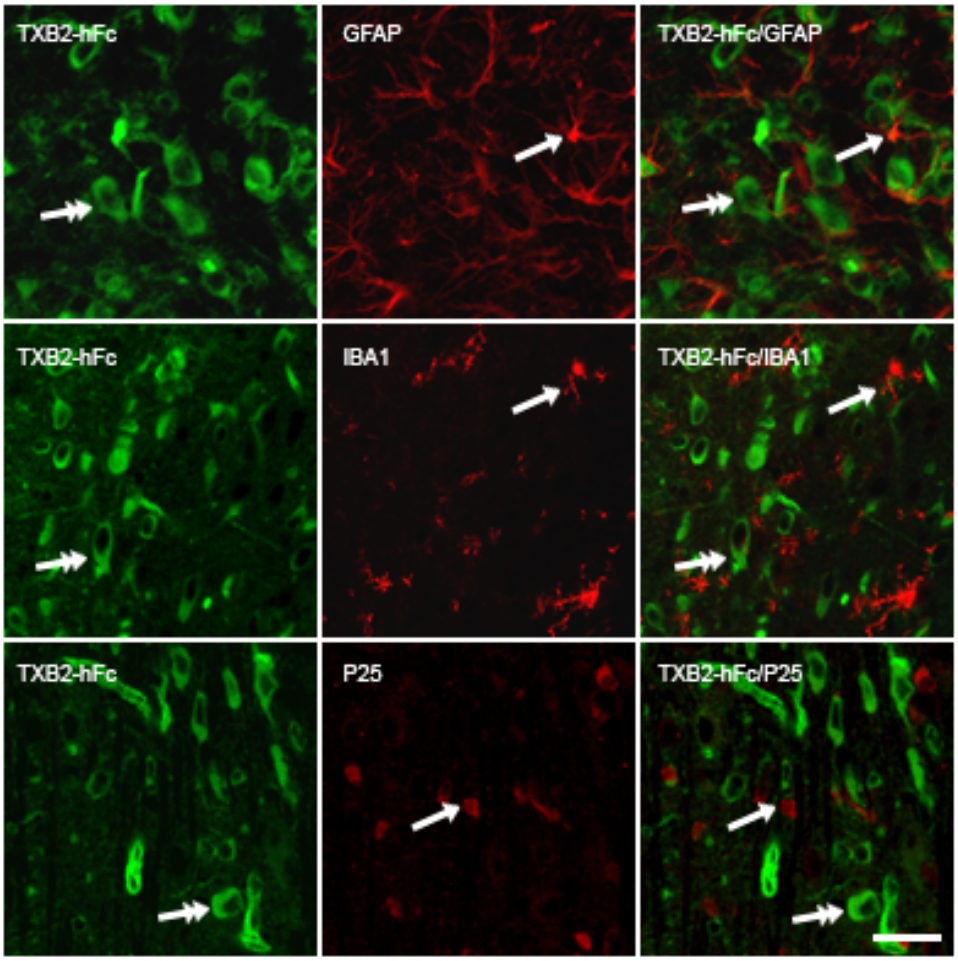

Figure S5. TXB2-hFc immunoreactivity is not confined to major glial cell types**.** Distribution of TXB2-hFc in brain evaluated taking a double-labelling approach to simultaneously detect the major glial cell types astrocytes (upper row), microglia (middle row), and oligodendrocytes (lower row) in high magnification. Sections taken from mesencephalon (astrocytes), lateral (microglia) and medial (oligodendrocytes) portions of the pons. The co-detection reveals that the various glial markers (red, single arrow) identifying numerous glial cells do not co-localize with TXB2-hFc (green, double-headed arrows). Scale bar: 80 µm.

Table S1

	OsX-3/4	in vitro R1	in vitro R2	in vivo R1	in vivo R2	in vivo R3
A	0	0	808	1163	1329	996
B	0	0	306	533	686	709
C	0	1	210	360	506	616
D	0	0	122	184	235	167
E	0	0	93	163	166	205
F	0	0	99	158	214	177
G	0	0	100	154	174	200
H	0	0	50	76	108	88
I	0	0	38	65	79	89
J	0	0	50	58	93	86
K	0	0	38	52	69	91
L	0	0	45	50	98	79
M	0	0	16	48	49	53
N	0	0	22	45	71	55
O	0	0	34	41	44	31
P	0	0	23	35	38	15
Q	0	0	22	35	36	19
R	0	0	13	33	67	71
S	0	0	16	32	45	46
T	0	0	10	30	45	62
U	0	0	9	30	42	64
V	0	0	10	28	36	24
W	0	0	23	26	40	21
X	0	0	17	26	43	48
Y	0	0	16	22	23	9
Z	0	0	18	20	55	57
AA	0	0	10	20	44	33
AB	0	0	1	13	37	50
AC	0	5	11	19	26	34

Table S1. The relative abundance of top 29 clones after selection by NGS. The VNAR sequences were grouped in families with common CDR3s. The 29 most abundant families are shown. Relative abundance was calculated as per million sequences at each stage of the selection.

Table S2

Analyte	hTfR1			mTfR1			rTfR1			cTfR1		
	ka (1/Ms)	kd (1/s)	KD (M)	ka (1/Ms)	kd (1/s)	KD (M)	ka (1/Ms)	kd (1/s)	KD (M)	ka (1/Ms)	kd (1/s)	KD (M)
A1-hFc	5.1E+4	8.6E-5	1.7E-9	4.7E+4	7.3E-5	1.5E-9	ND	ND	ND	4.9E+6	1.5E-3	3.1E-10
TXB2-hFc	2.2E+5	8.6E-5	3.9E-10	1.6E+5	1.0E-4	6.3E-10	1.0E+5	1.2E-4	1.2E-9	2.6E+5	7.4E-5	2.8E-10
Holo hTf	6.8E+4	4.6E-4	6.8E-9	ND	ND	ND	ND	ND	ND	ND	ND	ND
8D3-hFc	ND	ND	ND	4.1E+5	7.3E-5	1.8E-10	ND	ND	ND	ND	ND	ND
OKT9	1.5E+5	1.9E-5	1.3E-10	ND	ND	ND	ND	ND	ND	ND	ND	ND
OX26	ND	ND	ND	ND	ND	ND	7.7E+4	1.5E-4	2.0E-9	ND	ND	ND

Table S2. Binding kinetics to human, mouse, rat and cynomolgus monkey TfR1 (hTfR1, mTfR1, rTfR1 and cTfR1). All TfR1 construct ectodomains were expressed and purified in-house. SPR assays were performed using single cycle kinetics on an anti-His capture-chip coated with His-tagged TfR1 at 10 µg/ml. The association rate (ka), dissociation rate (kd) and binding affinity (KD) for TXB2-hFc and control VNAR-hFc were calculated. Holo hTf specific to human TfR1 as well as control antibodies were included with 8D3, OX26, and OKT9, specific to mouse, rat, human and human TfR1, respectively; not detected (ND).

REFERENCES

1. H. Kawabata, Transferrin and transferrin receptors update. *Free radical biology & medicine* **133**, 46-54 (2019).
2. P. M. Friden, L. R. Walus, G. F. Musso, M. A. Taylor, B. Malfroy, R. M. Starzyk, Anti-transferrin receptor antibody and antibody-drug conjugates cross the blood-brain barrier. *Proceedings of the National Academy of Sciences of the United States of America* **88**, 4771-4775 (1991).
3. K. B. Johnsen, A. Burkhart, L. B. Thomsen, T. L. Andresen, T. Moos, Targeting the transferrin receptor for brain drug delivery. *Progress in neurobiology* **181**, 101665 (2019).
4. J. A. Couch, Y. J. Yu, Y. Zhang, J. M. Tarrant, R. N. Fuji, W. J. Meilandt, H. Solanoy, R. K. Tong, K. Hoyte, W. Luk, Y. Lu, K. Gadkar, S. Prabhu, B. A. Ordonia, Q. Nguyen, Y. Lin, Z. Lin, M. Balazs, K. Scearce-Levie, J. A. Ernst, M. S. Dennis, R. J. Watts, Addressing safety liabilities of TfR bispecific antibodies that cross the blood-brain barrier. *Science translational medicine* **5**, 183ra157, 181-112 (2013).
5. W. M. Pardridge, R. J. Boado, D. J. Patrick, E. Ka-Wai Hui, J. Z. Lu, Blood-Brain Barrier Transport, Plasma Pharmacokinetics, and Neuropathology Following Chronic Treatment of the Rhesus Monkey with a Brain Penetrating Humanized Monoclonal Antibody Against the Human Transferrin Receptor. *Molecular pharmaceutics* **15**, 5207-5216 (2018).
6. H. J. Lee, B. Engelhardt, J. Lesley, U. Bickel, W. M. Pardridge, Targeting rat anti-mouse transferrin receptor monoclonal antibodies through blood-brain barrier in mouse. *The Journal of pharmacology and experimental therapeutics* **292**, 1048-1052 (2000).
7. R. J. Boado, Y. Zhang, Y. Wang, W. M. Pardridge, Engineering and expression of a chimeric transferrin receptor monoclonal antibody for blood-brain barrier delivery in the mouse. *Biotechnology and bioengineering* **102**, 1251-1258 (2009).
8. Y. J. Yu, Y. Zhang, M. Kenrick, K. Hoyte, W. Luk, Y. Lu, J. Atwal, J. M. Elliott, S. Prabhu, R. J. Watts, M. S. Dennis, Boosting brain uptake of a therapeutic antibody by reducing its affinity for a transcytosis target. *Science translational medicine* **3**, 84ra44 (2011).
9. N. Bien-Ly, Y. J. Yu, D. Bumbaca, J. Elstrott, C. A. Boswell, Y. Zhang, W. Luk, Y. Lu, M. S. Dennis, R. M. Weimer, I. Chung, R. J. Watts, Transferrin receptor (TfR) trafficking determines brain uptake of TfR antibody affinity variants. *The Journal of experimental medicine* **211**, 233-244 (2014).
10. J. Niewoehner, B. Bohrmann, L. Collin, E. Urich, H. Sade, P. Maier, P. Rueger, J. O. Stracke, W. Lau, A. C. Tissot, H. Loetscher, A. Ghosh, P. O. Freskgard, Increased brain penetration and potency of a therapeutic antibody using a monovalent molecular shuttle. *Neuron* **81**, 49-60 (2014).
11. D. Karaoglu Hanzatian, A. Schwartz, F. Gizatullin, J. Erickson, K. Deng, R. Villanueva, C. Stedman, C. Harris, T. Ghayur, A. Goodearl, Brain uptake of multivalent and multi-specific DVD-Ig proteins after systemic administration. *mAbs* **10**, 765-777 (2018).
12. C. I. Webster, J. Hatcher, M. Burrell, G. Thom, P. Thornton, I. Gurrell, I. Chessell, Enhanced delivery of IL-1 receptor antagonist to the central nervous system as a novel anti-transferrin receptor-IL-1RA fusion reverses neuropathic mechanical hypersensitivity. *Pain* **158**, 660-668 (2017).

13. G. Thom, M. Burrell, A. S. Haqqani, A. Yogi, E. Lessard, E. Brunette, C. Delaney, E. Baumann, D. Callaghan, N. Rodrigo, C. I. Webster, D. B. Stanimirovic, Enhanced Delivery of Galanin Conjugates to the Brain through Bioengineering of the Anti-Transferrin Receptor Antibody OX26. *Molecular pharmaceutics* **15**, 1420-1431 (2018).
14. R. L. Stanfield, H. Dooley, M. F. Flajnik, I. A. Wilson, Crystal structure of a shark single-domain antibody V region in complex with lysozyme. *Science (New York, N.Y.)* **305**, 1770-1773 (2004).
15. K. Griffiths, O. Dolezal, K. Parisi, J. Angerosa, C. Dogovski, M. Barraclough, A. Sanalla, J. L. Casey, I. González, M. A. Perugini, S. Nuttall, M. Foley, Shark Variable New Antigen Receptor (VNAR) Single Domain Antibody Fragments: Stability and Diagnostic Applications. *Antibodies* **2**, 66-81 (2013).
16. J. Hasler, J. L. Rutkowski. (US20170198281A1, 2015), vol. US20170198281A1.
17. D. Triguero, J. Buciak, W. M. Pardridge, Capillary depletion method for quantification of blood-brain barrier transport of circulating peptides and plasma proteins. *Journal of neurochemistry* **54**, 1882-1888 (1990).
18. M. Lo, H. S. Kim, R. K. Tong, T. W. Bainbridge, J. M. Vernes, Y. Zhang, Y. L. Lin, S. Chung, M. S. Dennis, Y. J. Zuchero, R. J. Watts, J. A. Couch, Y. G. Meng, J. K. Atwal, R. J. Brezski, C. Spiess, J. A. Ernst, Effector-attenuating Substitutions That Maintain Antibody Stability and Reduce Toxicity in Mice. *The Journal of biological chemistry* **292**, 3900-3908 (2017).
19. K. Kissel, S. Hamm, M. Schulz, A. Vecchi, C. Garlanda, B. Engelhardt, Immunohistochemical localization of the murine transferrin receptor (TfR) on blood-tissue barriers using a novel anti-TfR monoclonal antibody. *Histochemistry and cell biology* **110**, 63-72 (1998).
20. M. S. Ghandour, O. K. Langley, V. Varga, Immunohistological localization of gamma-glutamyltranspeptidase in cerebellum at light and electron microscope levels. *Neuroscience letters* **20**, 125-129 (1980).
21. T. Moos, Immunohistochemical localization of intraneuronal transferrin receptor immunoreactivity in the adult mouse central nervous system. *The Journal of comparative neurology* **375**, 675-692 (1996).
22. J. M. Hill, R. C. Switzer, 3rd, The regional distribution and cellular localization of iron in the rat brain. *Neuroscience* **11**, 595-603 (1984).
23. V. Ghetie, E. S. Ward, E. S. Vitetta, in *Handbook of Anticancer Pharmacokinetics and Pharmacodynamics*, W. D. Figg, H. L. McLeod, Eds. (Humana Press, Totowa, NJ, 2004), pp. 475-498.
24. M. Demeule, N. Beaudet, A. Regina, E. Besserer-Offroy, A. Murza, P. Tetreault, K. Belleville, C. Che, A. Larocque, C. Thiot, R. Beliveau, J. M. Longpre, E. Marsault, R. Leduc, J. E. Lachowicz, S. L. Gonias, J. P. Castaigne, P. Sarret, Conjugation of a brain-penetrant peptide with neurotensin provides antinociceptive properties. *The Journal of clinical investigation* **124**, 1199-1213 (2014).
25. E. Hermans, J. M. Maloteaux, Mechanisms of regulation of neurotensin receptors. *Pharmacology & therapeutics* **79**, 89-104 (1998).
26. R. Pasqualini, E. Ruoslahti, Organ targeting in vivo using phage display peptide libraries. *Nature* **380**, 364-366 (1996).
27. M. G. Kolonin, J. Sun, K. A. Do, C. I. Vidal, Y. Ji, K. A. Baggerly, R. Pasqualini, W. Arap, Synchronous selection of homing peptides for multiple tissues by in vivo phage

display. *FASEB journal : official publication of the Federation of American Societies for Experimental Biology* **20**, 979-981 (2006).
28. M. W. Smith, G. Al-Jayyoussi, M. Gumbleton, Peptide sequences mediating tropism to intact blood-brain barrier: an in vivo biodistribution study using phage display. *Peptides* **38**, 172-180 (2012).
29. C. C. Stutz, J. V. Georgieva, E. V. Shusta, Coupling Brain Perfusion Screens and Next Generation Sequencing to Identify Blood-Brain Barrier Binding Antibodies. *AIChE journal. American Institute of Chemical Engineers* **64**, 4229-4236 (2018).
30. E. Urich, R. Schmucki, N. Ruderisch, E. Kitas, U. Certa, H. Jacobsen, C. Schweitzer, A. Bergadano, M. Ebeling, H. Loetscher, P. O. Freskgard, Cargo Delivery into the Brain by in vivo identified Transport Peptides. *Scientific reports* **5**, 14104 (2015).
31. J. Li, L. Feng, X. Jiang, In vivo phage display screen for peptide sequences that cross the blood-cerebrospinal-fluid barrier. *Amino acids* **47**, 401-405 (2015).
32. X. M. Wan, Y. P. Chen, W. R. Xu, W. J. Yang, L. P. Wen, Identification of nose-to-brain homing peptide through phage display. *Peptides* **30**, 343-350 (2009).
33. A. Demogines, J. Abraham, H. Choe, M. Farzan, S. L. Sawyer, Dual host-virus arms races shape an essential housekeeping protein. *PLoS biology* **11**, e1001571 (2013).
34. T. Moos, E. H. Morgan, Restricted transport of anti-transferrin receptor antibody (OX26) through the blood-brain barrier in the rat. *Journal of neurochemistry* **79**, 119-129 (2001).
35. S. Paris-Robidas, V. Emond, C. Tremblay, D. Soulet, F. Calon, In vivo labeling of brain capillary endothelial cells after intravenous injection of monoclonal antibodies targeting the transferrin receptor. *Molecular pharmacology* **80**, 32-39 (2011).
36. G. Manich, I. Cabezon, J. del Valle, J. Duran-Vilaregut, A. Camins, M. Pallas, C. Pelegri, J. Vilaplana, Study of the transcytosis of an anti-transferrin receptor antibody with a Fab' cargo across the blood-brain barrier in mice. *European journal of pharmaceutical sciences : official journal of the European Federation for Pharmaceutical Sciences* **49**, 556-564 (2013).
37. A. Sugyo, A. B. Tsuji, H. Sudo, F. Nomura, H. Satoh, M. Koizumi, G. Kurosawa, Y. Kurosawa, T. Saga, Uptake of 111In-labeled fully human monoclonal antibody TSP-A18 reflects transferrin receptor expression in normal organs and tissues of mice. *Oncology reports* **37**, 1529-1536 (2017).
38. T. R. Daniels-Wells, M. L. Penichet, Transferrin receptor 1: a target for antibody-mediated cancer therapy. *Immunotherapy* **8**, 991-994 (2016).
39. Y. J. Yu, J. K. Atwal, Y. Zhang, R. K. Tong, K. R. Wildsmith, C. Tan, N. Bien-Ly, M. Hersom, J. A. Maloney, W. J. Meilandt, D. Bumbaca, K. Gadkar, K. Hoyte, W. Luk, Y. Lu, J. A. Ernst, K. Scearce-Levie, J. A. Couch, M. S. Dennis, R. J. Watts, Therapeutic bispecific antibodies cross the blood-brain barrier in nonhuman primates. *Science translational medicine* **6**, 261ra154 (2014).
40. J. Lesley, R. Schulte, J. Woods, Modulation of transferrin receptor expression and function by anti-transferrin receptor antibodies and antibody fragments. *Experimental cell research* **182**, 215-233 (1989).
41. J. Sun, R. J. Boado, W. M. Pardridge, R. K. Sumbria, Plasma Pharmacokinetics of High-Affinity Transferrin Receptor Antibody-Erythropoietin Fusion Protein is a Function of Effector Attenuation in Mice. *Molecular pharmaceutics* **16**, 3534-3543 (2019).
42. T. Moos, E. H. Morgan, Transferrin and transferrin receptor function in brain barrier systems. *Cellular and molecular neurobiology* **20**, 77-95 (2000).

43. R. Deane, W. Zheng, B. V. Zlokovic, Brain capillary endothelium and choroid plexus epithelium regulate transport of transferrin-bound and free iron into the rat brain. *Journal of neurochemistry* **88**, 813-820 (2004).
44. N. Strazielle, J. F. Ghersi-Egea, Potential Pathways for CNS Drug Delivery Across the Blood-Cerebrospinal Fluid Barrier. *Current pharmaceutical design* **22**, 5463-5476 (2016).
45. H. Y. Chang, K. Morrow, E. Bonacquisti, W. Zhang, D. K. Shah, Antibody pharmacokinetics in rat brain determined using microdialysis. *mAbs* **10**, 843-853 (2018).
46. W. C. Mustain, P. G. Rychahou, B. M. Evers, The role of neurotensin in physiologic and pathologic processes. *Current opinion in endocrinology, diabetes, and obesity* **18**, 75-82 (2011).
47. C. B. Nemeroff, G. Bissette, A. J. Prange, Jr., P. T. Loosen, T. S. Barlow, M. A. Lipton, Neurotensin: central nervous system effects of a hypothalamic peptide. *Brain research* **128**, 485-496 (1977).
48. E. Popp, A. Schneider, P. Vogel, P. Teschendorf, B. W. Bottiger, Time course of the hypothermic response to continuously administered neurotensin. *Neuropeptides* **41**, 349-354 (2007).